

On the rise of proton-proton cross-sections at high energies

D A Fagundes, M J Menon and P V R G Silva

Universidade Estadual de Campinas - UNICAMP, Instituto de Física Gleb Wataghin,
13083-859 Campinas, SP, Brazil

E-mail: fagundes@ifi.unicamp.br, menon@ifi.unicamp.br,
precchia@ifi.unicamp.br

Abstract. The rise of the total, elastic and inelastic hadronic cross sections at high energies is investigated by means of an analytical parametrization, with the exponent of the leading logarithm contribution as a free fit parameter. Using derivative dispersion relations with one subtraction, two different fits to proton-proton and antiproton-proton total cross section and rho parameter data are developed, reproducing well the experimental information in the energy region 5 GeV - 7 TeV. The parametrization for the total cross sections is then extended to fit the elastic (integrated) cross section data in the same energy region, with satisfactory results. From these empirical results we extract the energy dependence of several physical quantities: inelastic cross section, ratios elastic/total, inelastic/total cross sections, ratio total-cross-section/elastic-slope, elastic slope and optical point. All data, fitted and predicted, are quite well described. We find a statistically consistent solution indicating: (1) an increase of the hadronic cross sections with the energy faster than the log-squared bound by Froissart and Martin; (2) asymptotic limits $1/3$ and $2/3$ for the ratios elastic/total and inelastic/total cross sections, respectively, a result in agreement with unitarity. These indications corroborate recent theoretical arguments by Ya. I. Azimov on the rise of the total cross section.

PACS numbers: 13.85.-t, 11.10.Jj, 13.85.Lg

J. Phys. G: Nucl. Part. Phys. (2013)

1. Introduction

The rise of the hadron-hadron total, elastic and inelastic cross sections at high energies is an experimental fact. However, the exact energy dependence involved and a widely accepted theoretical explanation for this increase have been open problems for a long time. At present, these aspects constitute one of the greatest challenges for QCD, the gauge field theory of the strong interactions. The total cross section is connected with the forward *elastic amplitude* (optical theorem) and therefore, perturbative techniques cannot access the large distance phenomena that permeate the elastic channel. On the other hand, non-perturbative approaches are not yet able to evaluate *soft scattering states* from first principles. As a consequence, the dependence of the total hadronic cross section with the energy cannot yet be directly predicted by QCD.

In the phenomenological context, a wide variety of models present good descriptions of the available data. However, since they are characterized by distinct physical pictures [1, 2, 3, 4, 5, 6], not exclusively related to QCD, a global, unified and well accepted approach is still missing.

In the theoretical context, formal results from axiomatic local quantum field theory, general principles and further arguments, state that the total cross section cannot grow with the energy faster than log-squared [7, 8, 9], a result also extended to the inelastic cross section [10, 11, 12]. However, as recently discussed by Azimov [13, 14, 15], it is not obvious if these derivations can be directly applied to hadronic processes (QCD) and formal arguments suggest that the total cross section could grow faster than log-squared. Moreover, recent result from lattice QCD indicates an universal asymptotic logarithm-squared dependence for the hadronic total cross section, once some specific assumptions are made [16]. That is, this lattice QCD result does not represent a unique or exclusive solution.

In the experimental context, new results from the LHC and new estimates from the Pierre Auger Observatory for the proton-proton (pp) total cross sections are expected to shed light on the subject. In particular, the first result for the pp total cross section at 7 TeV (LHC) has been obtained by the TOTEM Collaboration, through a *luminosity-dependent measurement* [17]. Although, in principle, this is an experimental result considered rather conservative due to agreement with some model predictions, further investigations brought out some unexpected aspects. In fact, once included in amplitude analysis this point can not be adequately described by standard parametrization with leading log-squared dependence on the energy, as first discussed by us in [18] (hereafter referred to as FMS) and recently (2012) also indicated by the Particle Data Group [19]. In this respect, see Figure 46.10 in [19] (reviewed version on line): within the corresponding uncertainties, the $\ln^2(s)$ fit result lies below the high-precision TOTEM datum; see also "Note Added During Revision" in [18].

The main ingredient in the FMS analysis has been the use of an analytical parametrization introduced by Amaldi *et al* in the seventies [20] and also used by the UA4/2 Collaboration, in the nineties [21]. This parametrization is characterized

by power contributions at low energies (reggeons) and a leading contribution at high energies (pomeron), parametrized by a power law in the logarithm of the energy with the exponent as a free real parameter. Detailed analysis, with different methods and fit variants to total cross section data only, from pp and antiproton-proton ($\bar{p}p$) scattering above 5 GeV, led to the conclusion that the real exponent in the logarithmic term is statistically consistent with 2 if the TOTEM datum is not included in the analysis, but above 2 (around 2.2 - 2.3) if this point takes part in the fitted data-set.

In this work we extend the FMS analysis on pp and $\bar{p}p$ scattering above 5 GeV in several aspects, all of them including the result of the TOTEM Collaboration at 7 TeV.

1. As discussed in [18], since the analytical parametrization is nonlinear in several parameters, the data reductions demand start (feedback) values for the fit parameters [22] and depending on the choices the fit result may be different. Here, two different choices have been considered, one from the FMS analysis [18] and another one based on the recent results from the PDG [19].
2. Using derivative dispersion relations (DDR), we connect the total cross section, σ_{tot} , with the ρ parameter (ratio between the real and imaginary parts of the forward amplitude). With this analytical formalism, we first present the predictions for $\rho(s)$ from individual fits to σ_{tot} data and after that we develop novel simultaneous fits to σ_{tot} and ρ data. In both cases we discuss in some detail the important role of the subtraction constant, embodied in the dispersion relations.
3. As commented on above, the log-squared bound, originally stated for the total cross section by Froissart-Martin-Lukaszuk [7, 8, 9],

$$\sigma_{tot}(s) < \frac{\pi}{m_\pi^2} \ln^2 \left(\frac{s}{s_r} \right),$$

where s is the center-of-mass energy squared, s_r a constant, m_π the pion mass, has been recently extended to the inelastic cross section by Martin-Wu-Roy-Singh [10, 11, 12],

$$\sigma_{inel}(s) < \frac{1}{4} \frac{\pi}{m_\pi^2} \ln^2 \left(\frac{s}{s_r} \right).$$

Therefore, from s-channel unitarity, a similar bound is expected for the elastic (integrated) cross section, $\sigma_{el}(s)$. Based on the connection between the total cross section and the forward *elastic scattering amplitude* (optical theorem) and since the FMS analysis of the total cross section has indicated a power larger than 2, we address here the extension of the same parametrization to the *elastic cross section*. Namely, with start (feedback) values of the simultaneous fits to σ_{tot} and ρ data we develop new empirical fits to σ_{el} data, with the same analytical parametrization.

4. With the results from the empirical fits for $\sigma_{tot}(s)$, $\rho(s)$ and $\sigma_{el}(s)$, we present *predictions* for the energy dependence of several physical quantities: σ_{inel} , the ratios σ_{el}/σ_{tot} , $\sigma_{inel}/\sigma_{tot}$, the optical point, as well as a result for the ratio between σ_{tot} and the elastic slope B and from that for the proper slope B .

5. Here, all physical quantities that are compared with experimental data (fitted and predicted quantities), are displayed with uncertainty regions and are evaluated by means of standard (analytical) error propagation from the free fit parameters [22].

All the experimental data considered (fitted and predicted) are quite well described. Our analysis leads to solutions that favor an increase of the total and elastic cross sections faster than the log-squared bound. In that case, the violation of the bound does not imply in violation of unitarity, as recently discussed by Azimov. Indeed, we obtain that, asymptotically, $\sigma_{el}/\sigma_{tot} \rightarrow 1/3$ and $\sigma_{inel}/\sigma_{tot} \rightarrow 2/3$. However, although statistically consistent and corresponding to quite good descriptions of the existing data, our results do not constitute unique solutions, but possible solutions for the rise of the hadronic cross sections.

The manuscript is organized as follows. In section 2 we treat the fits to σ_{tot} and ρ data: the analytical parametrization for σ_{tot} is introduced and the analytical connection with ρ by means of dispersion relations is presented and discussed, with emphasis on the role of the subtraction constant. In section 3 the extension of the parametrization to elastic cross sections data is presented. In section 4 we display the predictions for the inelastic cross section, the ratios involving cross sections, the optical point, the elastic slope and compare with the corresponding experimental data, followed by discussions on each obtained result. Our conclusions and some critical remarks are the contents of section 5.

2. Total Cross Section and the Rho Parameter

At high energies, in terms of the *elastic* scattering amplitude F , the total cross section and the ρ parameter in the forward direction can be expressed by

$$\sigma_{tot}(s) = \frac{\text{Im } F(s, t = 0)}{s} \quad (\text{Optical theorem}) \quad (1)$$

$$\rho(s) = \frac{\text{Re } F(s, t = 0)}{\text{Im } F(s, t = 0)}, \quad (2)$$

where t is the four momentum transfer squared.

2.1. Experimental Data

Our interest here is the investigation of the high and asymptotic energy region, associated with particle-particle and antiparticle-particle scattering. For that reason we shall consider only elastic collisions with the *highest energy interval in terms of available data*, namely pp and $\bar{p}p$ scattering. With this restrictive choice we do not take into account data from other reactions, available only in the regions of intermediate and low energies or any constraint dictated by a supposed universal behavior.

The input data set for fits concerns *only accelerator data*, covering the region from 5 GeV up to 7 TeV. However, estimations of the pp total cross section from

cosmic-ray experiments will be displayed as illustrative results. The reason why we do not include this information in the fits is the model-dependence involved in the extraction of the proton-proton total cross section from proton-air production cross sections [23, 24, 25, 26]. The accelerator data on σ_{tot} and ρ from pp and $\bar{p}p$ scattering have been extracted from [17] and the PDG database [27], without any kind of data selection or sieve procedure. The estimations of the pp total cross sections from cosmic-ray experiments are from [27, 28]. All these data and estimations are exactly the same as that used and displayed in [18].

2.2. Analytical Parametrization

The analytical parametrization to be used here in the fits to pp and $\bar{p}p$ total cross sections data (and in section 3 to elastic cross sections data), is given by [18, 20, 21]

$$\sigma^{pp}(s) = a_1 \left[\frac{s}{s_l} \right]^{-b_1} - a_2 \left[\frac{s}{s_l} \right]^{-b_2} + \alpha + \beta \ln^\gamma \left(\frac{s}{s_h} \right), \quad (3)$$

$$\sigma^{\bar{p}p}(s) = a_1 \left[\frac{s}{s_l} \right]^{-b_1} + a_2 \left[\frac{s}{s_l} \right]^{-b_2} + \alpha + \beta \ln^\gamma \left(\frac{s}{s_h} \right), \quad (4)$$

where $s_l = 1 \text{ GeV}^2$ (fixed), a_1 , b_1 , a_2 , b_2 (low energies), α , β , γ and s_h (high energies) are, in general, free real fit parameters.

For the case of total cross section all the parameters above have specific physical interpretations in the context of the Regge-Gribov theory. They are associated with reggeon exchanges (first two terms) and pomeron exchanges (last two terms) at low and high energy regions, respectively [18, 29]. In the case of the elastic cross section we consider this parametrization as an empirical ansatz or as a representation.

2.3. Dispersion Relations and the Subtraction Constant

Amplitude analyses of the total cross section rising usually include the information on the ρ parameter through fits to both quantities [29, 30, 31, 32, 33, 34, 35, 36, 37, 38]. The connection between σ_{tot} and ρ is obtained by means of dispersion relations (integral and/or derivatives forms), or the asymptotic prescriptions for crossing even and odd amplitudes (Phragmén-Lindelöf theorem) [39, 40]. In the high-energy region, of interest in this work, the dispersion relations demand one subtraction [41, 42], which means the addition of one more free parameter in the simultaneous investigation of both quantities.

In the FMS analysis [18] the fits have been developed only with the σ_{tot} data, without the inclusion of the ρ information. Here, using DDR with one subtraction, we also treat simultaneous fits to both quantities. To this end, in this subsection, we shortly review some aspects related to integral and DDR, with emphasis on the origin and role of the subtraction constant. In the next subsections, we present our predictions for $\rho(s)$ from fits to σ_{tot} data and after that, we develop and discuss new simultaneous fits to ρ and σ_{tot} data.

2.3.1. Integral and Derivative Dispersion Relations Following the notation in [26], for pp and $\bar{p}p$ scattering, analyticity and crossing symmetry allow us to connect $\sigma_{tot}(s)$ and $\rho(s)$ through two compact and symmetric formulas:

$$\rho^{pp}(s)\sigma_{tot}^{pp}(s) = E(\sigma_+) + O(\sigma_-), \quad (5)$$

$$\rho^{\bar{p}p}(s)\sigma_{tot}^{\bar{p}p}(s) = E(\sigma_+) - O(\sigma_-), \quad (6)$$

where the even (+) and odd (−) cross section are related to the physical cross sections by

$$\sigma_{\pm}(s) = \frac{\sigma_{tot}^{pp} \pm \sigma_{tot}^{\bar{p}p}}{2}, \quad (7)$$

and $E(\sigma_+)$, $O(\sigma_-)$ are analytic transforms connecting the real and imaginary parts of crossing even and odd scattering amplitudes, respectively (associated with σ_+ and σ_-). These analyticity relations are usually expressed in an *integral* form (Hilbert transform [43]) and in the case of the forward direction the standard once-subtracted *integral dispersion relations* (IDR), with poles removed, may be expressed by [40, 41, 42, 44]

$$E_{int}(\sigma_+) \equiv \frac{K}{s} + \frac{2s}{\pi} P \int_{s_o}^{\infty} ds' \left[\frac{1}{s'^2 - s^2} \right] \sigma_+(s'), \quad (8)$$

$$O_{int}(\sigma_-) \equiv \frac{2}{\pi} P \int_{s_o}^{\infty} ds' \left[\frac{s'}{s'^2 - s^2} \right] \sigma_-(s'), \quad (9)$$

where K is the *subtraction constant* and P denotes principal value. We recall that in the even case, IDR with one and two subtractions are equal and in the odd case, those without subtraction and with one subtraction are also equal [40]. Therefore, with our parametrization of interest (3-4), the subtraction in the even part is adequate since, *asymptotically*, from equation (7), we have:

$$\sigma_+ \rightarrow \ln^{\gamma}(s) \quad \text{and} \quad \sigma_- \rightarrow 0 \quad \text{as} \quad \sqrt{s} \rightarrow \infty.$$

We shall return to the subject of the subtraction constant in the next subsection.

On the other hand, for classes of functions of interest, IDR can be replaced by derivative forms [45, 46, 47], known as *derivative dispersion relations* (DDR), which may be more useful for some practical calculations. In these formulas, differentiation with respect to the logarithm of the energy occurs in the argument of a trigonometric operator, as in the standard form deduced by Bronzan, Kane, and Sukhatme *in the high-energy approximation* ($s_0 \rightarrow 0$ in eqs. (8) and (9)) [48, 49]:

$$E_{der}(\sigma_+) \equiv \frac{K}{s} + \tan \left[\frac{\pi}{2} \frac{d}{d \ln s} \right] \sigma_+(s), \quad (10)$$

$$O_{der}(\sigma_-) \equiv \tan \left[\frac{\pi}{2} \left(1 + \frac{d}{d \ln s} \right) \right] \sigma_-(s), \quad (11)$$

corresponding, as before, to singly-subtracted DDR.

This completes the analytical approach: with an input parametrization for $\sigma_{tot}^{pp}(s)$, $\sigma_{tot}^{\bar{p}p}(s)$, eqs. (5), (6) and (7) allow, in principle, the determination of $\rho^{pp}(s)$ and $\rho^{\bar{p}p}(s)$ by means of either the IDR, (8) and (9), or the DDR, (10) and (11) in the high-energy approximation.

In our case, with the $\ln^\gamma(s/s_h)$ term and γ a free real parameter, IDR demand numerical methods and therefore a nonanalytic approach for error propagation from the fit parameters. The use of prescriptions seems to us unjustified in the region of intermediate and low energy data (5 - 20 GeV), since they are asymptotic results [39]. On the other hand, DDR allow an analytical approach and even the high-energy results, (10) and (11), can be applied in the low energy region, an effect related to the presence of the subtraction constant K . Since this effect plays a fundamental role in our analysis, let us first recall the origin, meaning and role of this constant, with focus on its disadvantages and *advantages in the present case*.

2.3.2. The Role of the Subtraction Constant Subtractions are useful tools to deal with the convergence of IDR and they are essentially based on a change of variable. In general grounds, suppose a given dispersion relation for a complex function $f(z)$ and let x_0 be some point on the real axis, at which $f(z)$ is analytic. The corresponding relation for $[f(z) - f(x_0)]/[z - x_0]$ leads to the subtracted dispersion relation [40, 43, 50]. Separating the real and imaginary parts of $f(z)$, the IDR for $\text{Re}f(z)$ includes now the constant $\text{Re}f(x_0)$, the subtraction constant. Therefore, in a particular physical problem it is necessary to determine $\text{Re}f(x_0)$ for some x_0 . For scattering amplitudes $x_0 \rightarrow s = 0$ is assumed, so that for an even amplitude (F_+), or cross section as in eq. (8), the subtraction constant reads

$$K = \text{Re } F_+(s = 0),$$

meaning the analytic continuation of the even amplitude at $s = 0$ [40].

Therefore, the subtraction constant has a well justified mathematical origin, related to the convergence of the integral. On the other hand, we cannot attribute to it a (real) physical meaning or value, since it is associated with the nonphysical region. However, in applying dispersion relations to connect σ_{tot} and ρ this constant appears explicitly and therefore must be taken into account. Note that to assume $K = 0$ is only a particular (and unjustified) choice, as any other. In this respect two disadvantages are in order to be recalled.

1. As an unknown constant, it plays the role of one more free parameter. However, the lack of a physical meaning contrasts with all the other free parameters present in the analytical parametrization of the total cross section, namely reggeons intercepts, reggeons strengths and leading pomeron contribution.

2. In data reductions, as a free parameter, its value affects the final values of the others physical free parameters. Moreover, it may seem that, once appearing in the form K/s in equations (8) and (10), its influence is limited to the low energy region. However, that is not true: typical (global) fits are characterized by *strong correlation among all free parameters*. That means K may affect the fit results even at high and asymptotic energies, as already discussed and demonstrated in [26, 49, 51].

Summarizing, once introduced in the fit procedure, one may, in principle, select and even anchor the outputs. That was one of the reasons why simultaneous fits, including the ρ information, were not considered in the FMS analysis (see however Appendix A in [18]).

On the other hand, *in applying DDR deduced in the high-energy approximation* (previous subsection), the subtraction constant develops a useful property, related to the equivalence between DDR and IDR. These aspects have been already demonstrated and discussed in [26, 49, 51] and in what follows we recall the main points.

As commented before, the DDR deduced by Bronzan-Kane-Sukhatme (10-11) have been obtained in the high-energy approximation, which means considering $s_0 \rightarrow 0$ in the lower limit of the IDR (8) and (9). Since for pp and $\bar{p}p$ scattering, $s_0 = 4m_p^2 \sim 3.5 \text{ GeV}^2$, it could be expected that, for a given parametrization, the results obtained by means of IDR with $s_0 = 4m_p^2$ fixed and through DDR are not the same. That, however, is not always the case. In [49] and references therein, the practical equivalence of IDR and DDR has been investigated in the case of the Donnachie-Landshoff parametrization, with both degenerate [52] and non-degenerate [31, 53] meson trajectories. Several variants have been considered in simultaneous fits to σ_{tot} and ρ data from pp and $\bar{p}p$ scattering: (i) energy cutoffs at 5 and 10 GeV; (ii) subtraction constant $K = 0$ and K as a free fit parameter; (iii) DDR and IDR with both $s_0 = 4m_p^2$ and $s_0 = 0$. In all cases, once the subtraction constant is used as a free parameter, the numerical results obtained through DDR (high-energy approximation) and IDR with fixed $s_0 = 4m_p^2$ (without the high-energy approximation) are the same, up to three significant figures in the fit parameters and χ^2/DOF (degrees of freedom). This effect is a consequence of the absorption of the high-energy approximation in an *effective* subtraction constant. Specifically, as analytically demonstrated in Sect. 4.4 of [49], the coefficient Δ of the series expansion associated with the integration from $s' = 0$ to $s' = 4m_p^2$ is absorbed by the subtraction constant, since the series can be put in the form

$$[K + \Delta] \frac{1}{s} + \mathcal{O}\left(\frac{1}{s^2}\right).$$

This effect of absorption of the high-energy approximation by the subtraction constant has also been confirmed by other authors [54, 55]. Therefore, despite the disadvantages of the subtraction constant, it can have here a useful practical or *pragmatic* role as a free fit parameter in the DDR: *it leads to the same result that could be obtained through the IDR without the high-energy approximation*.

We recall that, for classes of functions of interest in high-energy elastic scattering, DDR can be analytically extended down to 4 - 5 GeV [54, 56] or even below and for the whole energy interval (above the physical threshold), either in the form of a double infinity series, as first deduced by Ávila and Menon [57, 58], or in the form of a single series, as demonstrated by Ferreira and Sesma [59]. However it seems to us simpler here to consider the pragmatic role of the subtraction constant, since as explained above, with this constant as a free parameter the results obtained with the DDR (10) and (11) (high-energy approximation) are the same as those obtained through the IDR (8) and (9) (without the high-energy approximation). Therefore, let us focus on the DDR (10) and (11) with K as a free fit parameter.

2.3.3. Analytical results with Derivative Dispersion Relations The applicability of DDR in amplitude analysis has been critically reviewed by Ávila and Menon [49], in particular the replacement of the trigonometric operators in (10) and (11) by the corresponding series (see also [26]). In practice, with the presence of the $\ln^\gamma(s/s_h)$ term, the derivative transforms (10) and (11) can be evaluated through the operational expansion, introduced by Kang and Nicolescu [60] (see also section 3 in [49]):

$$E_{der}(\sigma_+) = \frac{K}{s} + \left[\frac{\pi}{2} \frac{d}{d \ln s} + \frac{1}{3} \left(\frac{\pi}{2} \frac{d}{d \ln s} \right)^2 + \frac{2}{15} \left(\frac{\pi}{2} \frac{d}{d \ln s} \right)^3 + \dots \right] \sigma_+(s), \quad (12)$$

$$\begin{aligned} O_{der}(\sigma_-) &= - \int \left\{ \frac{d}{d \ln s} \left[\cot \left(\frac{\pi}{2} \frac{d}{d \ln s} \right) \right] \sigma_-(s) \right\} d \ln s \\ &= - \frac{2}{\pi} \int \left\{ \left[1 - \frac{1}{3} \left(\frac{\pi}{2} \frac{d}{d \ln s} \right)^2 - \frac{1}{45} \left(\frac{\pi}{2} \frac{d}{d \ln s} \right)^4 - \dots \right] \sigma_-(s) \right\} d \ln s. \end{aligned} \quad (13)$$

With parametrization (3-4) as input and from (7), the evaluation of the power terms (low energy contribution) results in closed forms (sum of the series). For the logarithm term (leading contribution) a fast convergence is already obtained up to third order, since as we shall show $\gamma \sim 2.2 - 2.4$. In this case we obtain [18]

$$\begin{aligned} E_{der}(\sigma_+) &= \frac{K}{s} - a_1 \tan \left(\frac{\pi b_1}{2} \right) \left[\frac{s}{s_l} \right]^{-b_1} + \mathcal{A} \ln^{\gamma-1} \left(\frac{s}{s_h} \right) \\ &\quad + \mathcal{B} \ln^{\gamma-3} \left(\frac{s}{s_h} \right) + \mathcal{C} \ln^{\gamma-5} \left(\frac{s}{s_h} \right), \end{aligned} \quad (14)$$

where

$$\begin{aligned} \mathcal{A} &= \frac{\pi}{2} \beta \gamma, & \mathcal{B} &= \frac{1}{3} \left[\frac{\pi}{2} \right]^3 \beta \gamma [\gamma - 1][\gamma - 2], \\ \mathcal{C} &= \frac{2}{15} \left[\frac{\pi}{2} \right]^5 \beta \gamma [\gamma - 1][\gamma - 2][\gamma - 3][\gamma - 4] \end{aligned} \quad (15)$$

and for the odd contribution,

$$O_{der}(\sigma_-) = -a_2 \cot\left(\frac{\pi b_2}{2}\right) \left[\frac{s}{s_l}\right]^{-b_2}. \quad (16)$$

With the above results ((14),(15),(16)) and parametrization (3)-(4) for σ_{tot}^{pp} and $\sigma_{tot}^{\bar{p}p}$, equations (5) and (6) lead to the analytical expressions for $\rho^{pp}(s)$ and $\rho^{\bar{p}p}(s)$:

$$\begin{aligned} \rho^{pp}(s) = \frac{1}{\sigma_{tot}^{pp}(s)} & \left\{ \frac{K}{s} - a_1 \tan\left(\frac{\pi b_1}{2}\right) \left[\frac{s}{s_l}\right]^{-b_1} + \mathcal{A} \ln^{\gamma-1}\left(\frac{s}{s_h}\right) \right. \\ & \left. + \mathcal{B} \ln^{\gamma-3}\left(\frac{s}{s_h}\right) + \mathcal{C} \ln^{\gamma-5}\left(\frac{s}{s_h}\right) - a_2 \cot\left(\frac{\pi b_2}{2}\right) \left[\frac{s}{s_l}\right]^{-b_2} \right\}. \end{aligned} \quad (17)$$

and

$$\begin{aligned} \rho^{\bar{p}p}(s) = \frac{1}{\sigma_{tot}^{\bar{p}p}(s)} & \left\{ \frac{K}{s} - a_1 \tan\left(\frac{\pi b_1}{2}\right) \left[\frac{s}{s_l}\right]^{-b_1} + \mathcal{A} \ln^{\gamma-1}\left(\frac{s}{s_h}\right) \right. \\ & \left. + \mathcal{B} \ln^{\gamma-3}\left(\frac{s}{s_h}\right) + \mathcal{C} \ln^{\gamma-5}\left(\frac{s}{s_h}\right) + a_2 \cot\left(\frac{\pi b_2}{2}\right) \left[\frac{s}{s_l}\right]^{-b_2} \right\}, \end{aligned} \quad (18)$$

with \mathcal{A} , \mathcal{B} and \mathcal{C} given by eq. (15). Note that the analytical results imply that as $s \rightarrow \infty$:

$$\rho \propto \frac{1}{\ln s} \rightarrow 0,$$

which is in agreement with the rigorous asymptotic result by Khuri and Kinoshita [61].

2.4. Fits and Results

In this subsection, after discussing general aspects of the fit procedures and methodology, we present the results, through eqs. (17) and (18), of individual fits to σ_{tot} data with corresponding predictions for the $\rho(s)$ and those from simultaneous fits to σ_{tot} and $\rho(s)$ data. A detailed discussion of all the results obtained is presented in the next subsection.

2.4.1. Fit Procedures and Methodology. The nonlinearity of the fit (constants b_1 , b_2 , γ and s_h in equations (3)-(4)) demands a choice of the initial (feedback) values of the free parameters [22]. Here we shall address two different choices, denoted and explained in what follows.

Fit 1. In the FMS analysis, based only on the total cross section data, two ensembles, two methods and six variants have been tested for different feedback values and different fixed and free parameters. Here we shall select as a representative result with $\gamma > 2$ the one denoted in [18] as Ensemble $\sqrt{s}_{\max} = 7$ TeV, method 2 and variant 5 (table 4 and figure 6 in [18]). The reason for this choice is five-fold:

- (i) χ^2/DOF closest to 1;
- (ii) smaller relative error in the exponent γ ;

- (iii) result closest to the TOTEM point at 7 TeV;
- (iv) the numerical value of the exponent γ does not correspond to the largest or the smallest value obtained in the analysis figure 8 in [18]).
- (v) the reggeon intercepts, b_1 and b_2 , are fixed to 0.5, so that we can investigate the effects of this assumption (compared with fit 2 discussed below, in which the intercepts are not fixed).

Fit 2. The 2012 PDG analysis [19] is based on the highest rank parametrization result by the COMPETE Collaboration, introduced ten years ago [29, 30]. The functional form can be seen as a particular case of parametrization (3-4) in which the exponent γ is fixed to 2. The analysis by PDG includes different reactions and tests on the universality. Since this work corresponds to another fit result, with a kind of “conservative character” (namely $\gamma = 2$), we have considered the values of the parameters they have obtained as start values for fits with parametrization (3-4). We note that in doing so we are applying the parametrization to a subset of the data analyzed by the PDG and by the COMPETE Collaboration.

The data reductions have been performed with the objects of the class TMinuit of ROOT Framework [62] and all results correspond only to the cases of full convergence. As tests of goodness of fit we consider the χ^2 per DOF, with the χ^2 directly obtained from the MINUIT Code. In all fits we have adopted the Confidence Level (CL) of $\approx 68\%$ (one standard deviation), which means that the projection of the χ^2 distribution in $(N + 1)$ -dimensional space ($N =$ number of free fit parameters) contains 68 % of probability [22].

In the MINUIT Code, the correlation matrix gives a measure of the correlation between each pair of free parameters, with numerical limits ± 1 (full correlation) and 0 (no correlation) [22] (we shall return to this point in what follows). The error matrix provides the variances and covariances associated with each free parameter. This information is used in the analytic evaluation of the uncertainty regions in the fitted and extracted (predicted) physical quantities through standard error propagation procedures [22].

In what follows we shall address some of the points raised on the role of the subtraction constant in section 2.3.2, now with the results related to parametrization (3-4), fits 1 and 2 and the derivative dispersion results (17) and (18). First we treat the predictions for $\rho(s)$ from fits to σ_{tot} data and after that, simultaneous fits to both σ_{tot} and ρ data. As explained, the consistent applicability of the DDR demands the subtraction constant K as a free fit parameter. However, in order to illustrate some aspects of this constant we shall consider two variants in all cases: $K = 0$ and K as a free fit parameter.

2.4.2. Individual Fits to Total Cross Section Data and Predictions for the Rho Parameter

• Total Cross Section

In the case of fit 1, the values of the parameters obtained in [18], through

parametrization (3-4) and fit to only the total cross section data, are displayed in the second column of table 1 (σ_{tot} data column), with the corresponding statistical information on the data reduction. The dependences of the cross sections on energy are shown in figure 1, including uncertainty regions from error propagation, together with the experimental data analyzed (accelerator) and estimations of σ_{tot}^{pp} from cosmic-ray experiments.

In the case of fit 2 to total cross section data, the feedback values of the parameters and the fit results are displayed in the fifth and sixth columns of table 1, respectively (σ_{tot} data columns). In this case, the parameter s_M that appears associated with the power contributions in the PDG analysis, has been included in the reggeon strengths a_1 and a_2 . We distinguish however the scale factor in the logarithm contribution (s_h). The results for the total cross section, including uncertainty regions, and experimental information are shown in figure 2.

• Predictions for $\rho(s)$

From eqs. (17) and (18), any prediction for $\rho^{pp}(s)$ and $\rho^{\bar{p}p}(s)$ from the total cross section fit depends on the value of the subtraction constant. As commented before, we shall consider the two variants $K = 0$ and K as a free fit parameter to the ρ data. Specifically, we use as input the fixed values of the parameters for the total cross section (table 1), with $s_l = 1 \text{ GeV}^2$. For $K = 0$ (fixed) we obtain the direct prediction for $\rho(s)$. In the case of K as a free parameter we use $K = 0$ as start value and fit only the ρ data with this parameter, by fixing all the other parameters (from the total cross sections). In this case the first run with the MINUIT Code allows us to obtain the corresponding χ^2/DOF for $K = 0$. This statistical information and the values of K as fit parameter are displayed in the third and fourth columns of table 1 with fit 1 and seventh and eighth column of table 1 with fit 2 (ρ data columns). The dependences of ρ on energy, including uncertainty regions from error propagation and the experimental data, are shown in figure 1 with fit 1 and figure 2 with fit 2 (both for $K = 0$ and K as a free fit parameter).

2.4.3. Simultaneous Fits to Total Cross Section and Rho Data For simultaneous fits to σ_{tot} and ρ data, we have used as feedback the values of the parameters from fit 1 and fit 2 to σ_{tot} , displayed in table 1 (second and sixth columns). Here, we also consider the two variants: $K = 0$ and K as a free fit parameter (in this case, with $K = 0$ as start value). The fit results and statistical information are displayed in table 2. The results for $\sigma_{tot}(s)$ and $\rho(s)$ from fit 1 are shown in figures 3 ($K = 0$) and 4 (K as free parameter) and from fit 2 in figures 5 ($K = 0$) and 6 (K as free parameter).

2.5. Discussion and Partial Conclusions

Beyond the distinct start values for the parameters in Fits 1 and 2, an essential difference concerns the reggeon intercepts, which are fixed to $b_1 = b_2 = 0.5$ in the former case and

Table 1. Results of the individual fits to σ_{tot} data and the predictions for the ρ parameter, with the subtraction constant $K = 0$ and K as a free parameters and fits 1 and 2 (see text). The results denoted fit 1 (second, third and fourth columns) are those obtained in [18]. In fit 2 we use as initial values of the free parameters the central values from the PDG 2012 result [19] (fifth column) and our fit results are displayed in the sixth, seventh and eighth columns. Also included are the statistical information on the data reductions: degrees of freedom (DOF) and reduced χ^2 . The parameters a_1 , a_2 , α and β are in mb, s_h in GeV^2 and b_1 , b_2 , γ and K are dimensionless. In all cases, $s_l = 1.0 \text{ GeV}^2$ (fixed) in parametrization (3-4).

Ensemble:	Fit 1 [18]:				Fit 2:		
	σ_{tot} data	ρ data		Initial values	σ_{tot} data	ρ data	
		$K=0$	K free		Fit results [19]	$K=0$	K free
a_1	56.5 ± 1.1	—	—	46.06	60.2 ± 1.5	—	—
b_1	0.5 (fixed)	—	—	0.462	0.4850 ± 0.0079	—	—
a_2	27.70 ± 0.28	—	—	34.0	33.1 ± 1.7	—	—
b_2	0.5 (fixed)	—	—	0.550	0.540 ± 0.015	—	—
α	33.65 ± 0.22	—	—	34.71	31.52 ± 0.22	—	—
β	0.1301 ± 0.0086	—	—	0.265	0.0575 ± 0.0025	—	—
γ	2.213 ± 0.024	—	—	2.0	2.422 ± 0.016	—	—
s_h	3.90 ± 0.52	—	—	16.2	0.566 ± 0.065	—	—
K	—	0	44.8 ± 4.9	—	—	0	38.5 ± 4.9
DOF	158	76	75	—	156	76	75
χ^2/DOF	0.967	2.67	1.58	—	0.934	2.28	1.48

Table 2. Results of the simultaneous fits to σ_{tot} and ρ data, with feedback values from fit 1 and fit 2 (table 1), for $K = 0$ and K as a free fit parameter. Same legend as table 1.

	From Fit 1:		From Fit 2:	
	$K = 0$	K free	$K = 0$	K free
a_1	48.58 ± 0.72	51.5 ± 4.3	65.99 ± 0.55	59.8 ± 1.3
b_1	0.5 (fixed)	0.5 (fixed)	0.2758 ± 0.0026	0.4541 ± 0.0069
a_2	26.97 ± 0.27	27.63 ± 0.28	34.5 ± 1.5	34.1 ± 1.6
b_2	0.5 (fixed)	0.5 (fixed)	0.5511 ± 0.0094	0.547 ± 0.010
α	35.41 ± 0.15	35.16 ± 0.89	5.59 ± 0.24	29.78 ± 0.22
β	0.264 ± 0.041	0.32 ± 0.11	0.2575 ± 0.0028	0.0693 ± 0.0025
γ	2.018 ± 0.057	1.952 ± 0.098	1.8769 ± 0.0040	2.346 ± 0.013
s_h	18.7 ± 3.8	22 ± 15	0.00903 ± 0.00058	0.383 ± 0.041
K	0	41.2 ± 6.5	0	33.5 ± 5.9
DOF	232	231	232	231
χ^2/DOF	1.37	1.15	1.14	1.11

free in the latter. Based on this feature and the results presented in tables 1 and 2 and figures 1 - 6, we have the comments that follow, including some partial conclusions.

- Individual Fits to Total Cross Section Data and Predictions for the Rho Parameter (table 1, figures 1 and 2)

1. Both fits indicate $\gamma > 2$ with good statistical confidence (table 1):
fit 1: $\gamma \sim 2.21 \pm 0.02$ and $\chi^2/\text{DOF} \sim 0.97$,
fit 2: $\gamma \sim 2.42 \pm 0.02$ and $\chi^2/\text{DOF} \sim 0.93$.
2. The TOTEM result at 7 TeV is in agreement with the fits (fit 1 and fit 2) within uncertainties (figures 1 and 2).
3. In the predictions for the ρ parameter, the subtraction constant affects the results in the low energy region, $\sqrt{s} \lesssim 20$ GeV, essentially a change of curvature in $\rho^{\bar{p}p}$ around 10 GeV, in the case of K free (figures 1 and 2).
4. In all cases, the global description of the ρ data is quite good and, as expected, the best statistical results are obtained with K as a free fit parameter (table 1).
5. All the results with fit 2 corroborate those obtained in the FMS analysis.

- Simultaneous Fits to Total Cross Section and Rho Data (table 2 and figures 3 - 6)

1. Compared with individual fits to σ_{tot} data, the inclusion of ρ data in simultaneous fits leads to a decrease in the value of the exponent γ in all cases analyzed (tables 1 and 2):
fit 1: $\gamma \sim 2.21 \Rightarrow \gamma \sim 2.01$ ($K = 0$) and $\gamma \sim 1.95$ (K free)
fit 2: $\gamma \sim 2.42 \Rightarrow \gamma \sim 1.88$ ($K = 0$) and $\gamma \sim 2.35$ (K free)
2. The results with fit 1 are consistent with the log-squared bound (table 2):
 $\gamma \sim 2.02 \pm 0.06$ for $K = 0$ and $\gamma \sim 1.95 \pm 0.10$ for K free.
The lower error bar in the TOTEM datum is consistent with the upper uncertainty region of the fit result (figures 3 and 4).
3. The result with fit 2 for $K = 0$ is consistent with the log-squared bound, $\gamma \sim 1.877 \pm 0.0004$, but the fit uncertainty region does not reach the error bar of the TOTEM datum at 7 TeV (figure 5).
4. The result with fit 2 for K free is consistent with an increase of the total cross section faster than the log-squared bound, $\gamma \sim 2.35 \pm 0.01$ and the lower error bar of the TOTEM datum is in agreement with the fit result within uncertainties (figure 6).

As commented before, we have included the results with $K = 0$ only to illustrate some aspects of the subtraction constant, outlined above. Since the formal and consistent applicability of the DDR here used demands the subtraction constant as a free fit parameter, we shall focus our partial conclusions on this case only.

Concerning fit 1, we understand that fixing the reggeon intercepts to 0.5, results in a substantial constraint in the possible increase of the total cross section, when

the ρ data is included in simultaneous fits. That is a consequence of the correlations among all the fit parameters, in particular those involving K , s_h and γ . On the other hand, with fit 2, the reggeon intercepts and strengths are free to control the low and intermediate energy data, leaving the parameters associated with the constant and the leading logarithmic contributions adequately applied to the highest energy data. The correlation coefficients for both fits with K as a free fit parameter are displayed in Appendix A, where the correlations among K , s_h and γ are stressed. Moreover, fit 2 results in a χ^2/DOF closest to 1 and within the uncertainty regions all the experimental information on σ_{tot} and ρ is well described (figure 6).

In addition, note that for gamma real (not an integer) the logarithm term $\ln^\gamma(s/s_h)$ is not defined for $s < s_h$ and that our energy cutoff is fixed at $s_{min} = 25 \text{ GeV}^2$. In the case of fit 1, $s_h = 22 \pm 15 \text{ GeV}^2$ reaches the physical region (above the energy cutoff) within the uncertainty, leading, therefore, to a questionable result. That, however, is not the case with fit 2 because $s_h = 0.38 \pm 0.04 \text{ GeV}^2$.

Based on these facts, we shall select as our representative result that obtained with fit 2 in the simultaneous fits to σ_{tot} and ρ data in the case of K as a free fit parameter (fifth column in table 2). This result, as well as those obtained with individual fits to σ_{tot} data (fits 1 and 2) support an increase of the total cross section faster than the log-squared bound.

3. Fits to Elastic Cross Section Data

From s-channel unitarity, an increase of the total cross section faster than log-squared is expected to be, in some way, connected with a similar effect in the elastic and/or inelastic cross sections. At least that is what is suggested by the log-squared bound of the total cross section, recently extended to the inelastic cross section, as recalled in our introduction. Therefore, to go one step further, a point of interest is to test the applicability of the same parametrization (3-4) to the elastic or inelastic cross section data. In order to address this possibility we shall consider only the *elastic cross section* for the four reasons that follow.

- (i) From the optical theorem the total cross section is connected with the *elastic amplitude* in the forward direction.
- (ii) Total and elastic cross sections can be directly measured or estimated without the need of model assumptions. That however is not the case for the inelastic cross section due to the single and double dissociative contributions.
- (iii) The least ambiguous way to estimate the inelastic cross section is from unitarity, namely $\sigma_{inel} = \sigma_{tot} - \sigma_{el}$ [63], which suggests a more fundamental character for the last two quantities.
- (iv) To select a statistically consistent ensemble of σ_{inel} data for fit is not an easy task due to both model-dependence in “direct” estimations and the different data from

Table 3. Results of the fit to σ_{el} data through parametrization (3-4), with feedback values from fit 2, K free (fifth column in table 2). Same legend as table 1.

a_1	30.7 ± 3.6
b_1	0.551 ± 0.037
a_2	0.236 ± 0.071
b_2	0.134 ± 0.012
α	4.28 ± 0.14
β	0.02358 ± 0.00054
γ	2.346 (fixed)
s_h	0.978 ± 0.023
DOF	97
χ^2/DOF	1.62

different experiments and energies for σ_{tot} and σ_{el} , if using unitarity.

The experimental data on the elastic cross section from pp and $\bar{p}p$ scattering have been extracted from the PDG database [27], without any kind of data selection or sieve procedure. For the fits to the elastic cross section data with parametrization (3-4) we have used as start values those obtained with our representative result: fit 2 and K as a free fit parameter in the simultaneous fits to σ_{tot} and ρ data.

In this case, a crucial point concerns the exponent γ that controls the asymptotic behavior of the cross sections. Given that we have obtained for the total cross section $\gamma_{tot} = 2.346 \pm 0.013$, a value different from this for the elastic cross section, γ_{el} , has no physical meaning, due to direct violation of unitarity by the ratio σ_{el}/σ_{tot} or the reduction of this ratio to zero at asymptotic energies. Therefore we shall *explore the possibility that the same exponent applies for the elastic cross section* as well. Specifically, we fix this parameter to the central value obtained for the total cross section, $\gamma_{el} = 2.346$. With the above assumptions and fit procedures, we obtain the results displayed in table 3 and figure 7, corresponding therefore to a good reproduction of the experimental data. We shall discuss this result together with predictions for other physical quantities in the next section.

4. Predictions for Other Physical Quantities

Based on the empirical fits developed for $\sigma_{tot}(s)$, $\rho(s)$ and $\sigma_{el}(s)$, we present here the predictions for several physical quantities, followed by a discussion on each result.

4.1. Inelastic Cross Section and Ratios Elastic/Total and Inelastic/Total

From unitarity, by subtracting parametrization (3-4) with the corresponding values of the parameters displayed in table 2 for $\sigma_{tot}(s)$ and table 3 for $\sigma_{el}(s)$, we obtain our predictions for $\sigma_{inel}(s)$. The result is shown in figure 8 together with the experimental data [27, 64, 65, 66] and the uncertainty region. With this result and those for $\sigma_{tot}(s)$

and $\sigma_{el}(s)$, we extract the corresponding predictions for the ratios σ_{el}/σ_{tot} and $\sigma_{inel}/\sigma_{tot}$, displayed in figures 9 and 10, respectively.

4.2. Optical Point, Elastic Slope and the Ratio with the Total Cross Section

In this section we first recall the definitions of the elastic slope B , the optical point and an expression connecting the ratios σ_{el}/σ_{tot} and σ_{tot}/B . After that we present our predictions.

In terms of the elastic amplitude, the differential cross section is expressed by

$$\frac{d\sigma}{dt}(s, t) = \frac{1}{16\pi s^2} |F(s, t)|^2, \quad (19)$$

and the *slope* of the elastic differential cross section in the forward direction is defined as

$$B(s, t=0) = \left[\frac{d}{dt} \left(\ln \frac{d\sigma}{dt} \right) \right]_{t=0}. \quad (20)$$

From (1), (2) and (19), the *optical point* is given by

$$\left. \frac{d\sigma}{dt} \right|_{t=0} = \frac{\sigma_{tot}^2 [1 + \rho^2]}{16\pi}. \quad (21)$$

The integrated elastic cross section reads

$$\sigma_{el}(s) = \int_{t_0}^0 \frac{d\sigma}{dt}(s, t) dt, \quad (22)$$

where t_0 defines the physical (kinematic) region.

Concerning the differential cross section, experimental data indicate a sharp forward peak, followed by a dip-bump or dip-shoulder structure above $\sim 0.5 \text{ GeV}^2$ (Tevatron, LHC). Typically, these structures are located more than 5 decades below the optical point, equation (21). These experimental facts are important in the determination of the integrated elastic cross section, since in this case the differential cross section can effectively be represented by an exponential fall off, simulated by a model-independent parametrization [17],

$$\frac{d\sigma}{dt} = \left. \frac{d\sigma}{dt} \right|_{t=0} e^{Bt}, \quad (23)$$

with B the (constant) forward slope. In that case, by assuming $t_0 \rightarrow -\infty$ in eq. (22), the integrated elastic cross section is given by the approximate result

$$\sigma_{el}(s) = \frac{1}{B(s)} \frac{\sigma_{tot}^2(s)}{16\pi} [1 + \rho^2]$$

and therefore,

$$\frac{\sigma_{tot}(s)}{B(s)} = \frac{16\pi}{[1 + \rho^2]} \frac{\sigma_{el}(s)}{\sigma_{tot}(s)}, \quad (24)$$

which is very close to the MacDowell-Martin bound [67],

$$\frac{\sigma_{tot}(s)}{B(s)} \leq 18\pi \frac{\sigma_{el}(s)}{\sigma_{tot}(s)}, \quad (25)$$

a result recently discussed in more detail in [68]. For our purposes, the main ingredient in the result (24) is the possibility to investigate the behavior of $\sigma_{tot}(s)/B(s)$ from the information on the ratio $\sigma_{el}(s)/\sigma_{tot}(s)$ (see also [68]).

With our empirical results for $\sigma_{tot}(s)$, $\rho(s)$ and $\sigma_{el}(s)$ we can predict the optical point (21), the ratio σ_{tot}/B (24) and from that the elastic slope B . The results for the last two quantities are shown in figures 11 and 12, respectively (experimental information on the slope parameter B has been compiled from the Durham database [69]).

The predictions for several quantities of interest at 7, 8, 14 and 57 TeV are displayed in table 4, together with the TOTEM results at 7 TeV.

Table 4. TOTEM results at 7 TeV and predictions for several physical quantities associated with the pp elastic scattering at the LHC and Pierre Auger Observatory energies.

Physical quantity	7 TeV TOTEM [17]	7 TeV	8 TeV	14 TeV	57 TeV
σ_{tot} (mb)	98.3 ± 2.8	96.40 ± 0.97	98.7 ± 1.0	108.6 ± 1.2	137.0 ± 1.9
ρ	-	0.1362 ± 0.0016	0.1357 ± 0.0016	0.1333 ± 0.0015	0.1261 ± 0.0013
σ_{el} (mb)	24.8 ± 1.2	24.31 ± 0.31	25.03 ± 0.33	28.18 ± 0.39	37.26 ± 0.59
σ_{inel} (mb)	73.5 ± 3.1	72.1 ± 1.0	73.7 ± 1.1	80.4 ± 1.3	99.7 ± 2.0
σ_{el}/σ_{tot}	0.252 ± 0.014	0.2522 ± 0.0041	0.2536 ± 0.0042	0.2595 ± 0.0046	0.2720 ± 0.0057
$\sigma_{inel}/\sigma_{tot}$	0.7477 ± 0.038	0.7478 ± 0.0041	0.7465 ± 0.0042	0.7405 ± 0.0046	0.7280 ± 0.0057
σ_{tot}/B	12.56 ± 0.43	12.44 ± 0.21	12.51 ± 0.21	12.82 ± 0.23	13.46 ± 0.28
B (GeV ⁻²)	20.10 ± 0.36	19.89 ± 0.39	20.25 ± 0.40	21.76 ± 0.46	26.15 ± 0.66
$d\sigma/dt _{t=0}$ (mbGeV ⁻²)	504 ± 27	483.6 ± 9.7	507 ± 10	613 ± 14	974 ± 27

4.3. Discussion

From figure 8 the prediction for $\sigma_{inel}(s)$ presents good agreement with all the accelerator data and, within the uncertainty, also with the upper error bar of the Auger result at 57 TeV. At 7 TeV it favors the TOTEM datum, a result obtained through unitarity and therefore corresponding to a model-independent evaluation.

The results for the ratios of elastic/total and inelastic/total cross sections are displayed in figures 9 and 10. Within the uncertainty region, the predictions are also consistent with the TOTEM results at 7 TeV. These results lead to the consequences that follows.

Asymptotically ($s \rightarrow \infty$), from parametrization (3-4) and by denoting the parameters associated with σ_{tot} and σ_{el} fits by the corresponding indexes, we have

$$\frac{\sigma_{el}}{\sigma_{tot}} \rightarrow \frac{\beta_{el}}{\beta_{tot}} \quad \text{and} \quad \frac{\sigma_{inel}}{\sigma_{tot}} \rightarrow 1 - \frac{\beta_{el}}{\beta_{tot}}.$$

From tables 2 and 3 we obtain

$$\frac{\sigma_{el}}{\sigma_{tot}} \rightarrow 0.340 \pm 0.015 \quad \text{and} \quad \frac{\sigma_{inel}}{\sigma_{tot}} \rightarrow 0.660 \pm 0.015,$$

which are consistent with the rational limits:

$$\frac{\sigma_{el}}{\sigma_{tot}} \rightarrow \frac{1}{3} \quad \text{and} \quad \frac{\sigma_{inel}}{\sigma_{tot}} \rightarrow \frac{2}{3}, \quad (26)$$

indicating, therefore, a constant asymptotic value for the ratio σ_{el}/σ_{tot} which lies below 1/2, the black-disc limit.

It is interesting to note that the above results corroborate recent arguments attributing the black-disc limit to a combination of the soft processes, namely elastic and diffractive. Specifically, denoting σ_{diff} the single and double diffractive contributions, Grau-Pacetti-Pancheri-Srivastava have proposed the following asymptotic limit [70]

$$\frac{\sigma_{el}}{\sigma_{tot}} + \frac{\sigma_{diff}}{\sigma_{tot}} \rightarrow \frac{1}{2} \quad \text{as} \quad s \rightarrow \infty.$$

This argument is based on the formulation of eikonal models [63, 71] and according to our results it is expected:

$$\frac{\sigma_{diff}}{\sigma_{tot}} \rightarrow \frac{1}{6}.$$

Another aspect concerns the recently proposed empirical parametrization for the ratio elastic/total cross section by Fagundes and Menon [68],

$$\frac{\sigma_{el}}{\sigma_{tot}}(s) = A \tanh(\gamma_1 + \gamma_2 \ln s + \gamma_3 \ln^2 s), \quad (27)$$

where γ_i , $i = 1, 2, 3$ are free fit parameters and A represents the asymptotic limit. In this work the authors have considered two extrema cases, $A = 1/2$ (black-disc limit) and $A = 1$ (beyond the black-disc limit), with good descriptions of the pp data above 10 GeV. Our rational limit (26) implies $A = 1/3$ and therefore another scenario, lying asymptotically below the black-disc limit, as already pointed out.

The predictions for the ratio σ_{tot}/B through equation (24) and for the elastic slope B are displayed in figures 11 and 12, respectively. We recall that, even in the forward direction ($t = 0$), the determination of the slope from the differential cross section data demands some interval in the momentum transfer. That can explain some of the discrepant points in both figures since the corresponding intervals from different experiments are not always the same. Within the uncertainty regions, the predictions show good agreement with the experimental information at high energies, specially

with the TOTEM result at 7 TeV. Asymptotically, from eq. (24) and since $\rho \rightarrow 0$ (section 2.3.3), our rational limit (26) gives

$$\frac{\sigma_{tot}}{B} \rightarrow \frac{16\pi}{3}$$

and therefore, an asymptotic increase of the slope also faster than log-squared. As commented before, this result represents a different scenario from that discussed in [68] and also in [72].

In table 4 we display our numerical results (with uncertainties) for all the physical quantities here discussed and at different energies of interest in present and future experiments. At 7 TeV, except for the ρ parameter not determined by the TOTEM Collaboration, the compatibility of our results with the experimental data is quite good, for all physical quantities.

At last, another aspect deserving some comments concerns the predictions for the proton-proton total cross sections beyond the (accelerator) energy region analyzed, namely the estimations of σ_{tot}^{pp} from proton-air production cross section in cosmic-ray experiments. As already commented, these points did not take part in our data reductions and have been displayed only as qualitative illustrations. The estimations at the highest energies (Fly's Eye and Auger Collaborations) depend on extrapolation from phenomenological models tested only in the accelerator energy region. This fact, associated with the relative small cosmic-ray flux above ~ 20 TeV, results in extremely large uncertainties, as shown in our figures. Even though, the fit extrapolation suggests good agreement with these points (figure 6), in particular our numerical prediction at 57 TeV (table 4) with the recent Auger Collaboration estimation for the total cross section, $\sigma_{tot}^{pp} = [133 \pm 13 \text{ (stat)}_{-20}^{+17} \text{ (sys)} \pm 16 \text{ (Glauber)}] \text{ mb}$ [28]. However, it is important to note that systematic and theoretical (Glauber) uncertainties are equally likely quantities, that is, do not follow Gaussian distributions, as is the case of statistical uncertainties. That means the above central value is equally likely to lie in any place limited by the corresponding non-statistical uncertainties. For example, added in quadrature the resulting uncertainty corresponds to ≈ 23 mb (around 17 % of the central value). This result contrasts with the small systematic uncertainty of the TOTEM point at 7 TeV, namely 2.8 mb (around 2.8 %). Therefore, despite the suggestive global agreement, the large equally likely uncertainty may imply in different scenarios, as already discussed in [17]. We add that this observation puts limits on recent arguments by Block and Halzen in what concerns the description of the Auger Collaboration result quoted above [73] (see also our critical remarks at the end of the next section).

5. Conclusions and Critical Remarks

In this work an amplitude analysis on the forward pp and $\bar{p}p$ elastic scattering in the energy region 5 GeV - 7 TeV has been presented. The main point concerns the investigation of the log-squared bound in the rise of the cross sections with the energy. To address this question, an analytical parametrization introduced by Amaldi *et al* [20],

with the exponent of the leading logarithm contribution as a free fit parameter, has been used. Analytical connection between σ_{tot} and ρ parameter has been obtained by means of subtracted DDR. The presentation has been divided in three parts: (1) individual and simultaneous fits to σ_{tot} and ρ data, with focus on the role of the subtraction constant; (2) extension of the parametrization to the elastic cross section data with fixed exponent of the logarithm contribution; (3) predictions for other physical quantities and the study of some consequences.

As we have shown and discussed in detail all analyzed and predicted data are quite well described. The results indicate: (i) an increase of the hadronic cross sections faster than the log-squared bound; (ii) asymptotic limits for the ratios elastic/total and inelastic/total cross sections consistent with $1/3$ and $2/3$, respectively. Therefore, the violation of the bound does not imply in violation of unitarity, as recently discussed by Azimov: the fast rise may correspond to a rapid high-energy increase of the scattering amplitude in non-physical regions [13, 14].

The possible rise of the total cross section faster than the log-squared of s may seems an unexpected result. However, that is not the case *in what concerns the use of parametrization* (3-4), namely the possibility to treat γ as a free parameter and not to fix it to 2 (or 1). In fact, up to our knowledge, before the FMS analysis, this parametrization was used in two works only, the first one by Amaldi *et al* in the seventies and the second by the UA4/2 Collaboration in the nineties. Both analyses treated only pp and $\bar{p}p$ elastic scattering and simultaneous fits to σ_{tot} and ρ data. In the energy interval $5 \text{ GeV} < \sqrt{s} \leq 62.5 \text{ GeV}$, Amaldi *et al* obtained [20]

$$\gamma = 2.10 \pm 0.10$$

and the UA4/2 Collaboration, with the data set extended up to 546 GeV [21],

$$\gamma = 2.25^{+0.35}_{-0.31}.$$

These results, well known for a long time, indicate the possibility of a rise of the total cross section faster than the log-squared bound.

In the FMS analysis two ensembles on σ_{tot} data have been tested, one with data up to $\sqrt{s}_{max} = 1.8 \text{ TeV}$ and another one including the TOTEM result, namely $\sqrt{s}_{max} = 7 \text{ TeV}$. The novel aspect of the analysis consisted in the evidence that with the former ensemble the γ value is consistent with 2, but above 2 with the latter one. In the case of $\sqrt{s}_{max} = 7 \text{ TeV}$, several solutions have been obtained with different methods and variants [18]:

$$\gamma \approx 2.10 \pm 0.03 \text{ (method 1, variant 1)}, \quad \gamma \approx 2.27 \pm 0.04 \text{ (method 1, variant 3)},$$

$$\gamma \approx 2.21 \pm 0.02 \text{ (method 2, variant 5)}, \quad \gamma \approx 2.10 \pm 0.11 \text{ (method 2, variant 6)}.$$

Although the fits had been restricted to σ_{tot} data only, the use of DDR led to predictions for the ρ parameter consistent with the experimental information, even with the largest γ values [18]. Here, we have obtained with fit 2 to σ_{tot} data

$$\gamma \approx 2.42 \pm 0.02$$

and in the case of simultaneous fits to σ_{tot} and ρ data,

$$\gamma \approx 2.35 \pm 0.01.$$

Therefore, based on all the above results, we understand as evident the fact that parametrization (3-4) applied to experimental data may lead to statistically consistent solutions with $\gamma > 2$, possibly in the interval 2.2 - 2.4.

The leading contribution in parametrizations of the total cross section is expected to be associated with pomeron exchanges [1, 2]. For $\gamma = 1$, the constant plus $\ln s$ terms correspond to a double pole at $J = 1$ and for $\gamma = 2$ a triple pole (expressed by $\ln^2 s$, $\ln s$ and the constant terms) [29, 44]. The case of non-integer exponent, with $0 < \gamma < 2$ corresponds to a strong-coupling scenario [74, 75] and a fractional power, $\gamma = 3/2$ (in general $1 < \gamma < 2$), is phenomenologically indicated by the eikonal minijet model with soft gluon k_t -resummation [63, 70, 76, 77]. Presently, we do not have a physical interpretation for a leading logarithm contribution with the exponent γ as a real parameter greater than 2. Perhaps thinking about an effective exponent, representing the sum of different contributions might not be so speculative.

Once associated with the leading contribution in parametrization (3-4), the γ value from data reductions is essentially determined by the experimental information at the highest energy interval available. With $\sqrt{s}_{max} = 1.8$ TeV we are faced with the well known discrepant values of σ_{tot} obtained by the CDF, E710 and E811 Collaborations. This set of data gives no practical information on the rise of the total cross section, except for a possible effective mean value in data reductions. It seems peculiar the fact that most phenomenological models and even amplitude analyses present consistence with this *imaginary* mean value. On the other hand, compared with all the experimental data available, the TOTEM results at 7 TeV are characterized by extremely small uncertainties, as can be easily seen in the figures. Our analysis has been essentially based on fits to total cross section and elastic cross section, for which the uncertainties in the TOTEM data are around 2.8 % and 4.8 %, respectively. Therefore, in our data reductions, with the reduced χ^2 as a test of goodness of fit, these two points have played an essential role in the determination of the γ parameter. In other words, we understand that our results indicating $\gamma > 2$ are consequences of the TOTEM results at 7 TeV, as also discussed in [18]. The 2012 PDG analysis corroborates this conclusion since, as already commented in our introduction, with the updated dataset the COMPETE log-squared parametrization does not describe the TOTEM datum (Figure 46.10 in [19]); see also our recent discussion [78], section III.A, specially Figure 1 in that paper.

It should be also noted that, contrasting with an effective violation of the Froissart-Martin bound, a rise of σ_{tot} faster than log-squared of s at the LHC energy region, may be associated with some local effect, so that, asymptotically the bound remains valid. In that case, however, our asymptotic results, in particular those concerning the ratios between elastic/inelastic and total cross sections may have no meaning.

Therefore, based on the above critical comments, we understand that further measurements on the total and elastic cross sections at the LHC energy region are

necessary before any firm conclusion can be drawn on the γ value and consequently on the results here presented and discussed. We also emphasize that our results represent possible consistent statistical solutions for the behavior of the total cross section, but do not correspond to unique solutions. Despite these strong limitations, we hope this analysis and our previous work [18] might contribute with further interpretations and developments in the investigation of the rise of the hadronic cross sections at high energies, a problem, in our opinion, still unsolved.

Note added

After this analysis was completed, new high-precision measurements of the total cross section at 7 and 8 TeV have been reported by the TOTEM Collaboration [79, 80, 81]. An updated analysis, using the analytical parametrizations (1-5) and including in the data set all these new measurements have been developed by Menon and Silva [82]. The obtained results on the rise of the total cross section at high energy corroborate those presented here.

Acknowledgments

We are thankful to C. Dobrigkeit for a critical reading of the manuscript and useful discussions. Research supported by FAPESP (Contracts Nos. 11/15016-4, 11/00505-0, 09/50180-0).

Appendix A. Correlation Matrices

In the MINUIT code the symmetric correlation matrix provides a measure of the correlation between each pair of free parameter through a coefficient with numerical limits ± 1 (full correlation) and 0 (no correlation) [22, 62]. The results from fits 1 and 2 are displayed in table A1.

References

- [1] V. Barone and E. Predazzi, *High-Energy Particle Diffraction* (Spring-Verlag, Berlin, 2002).
- [2] S. Donnachie, G. Dosch, P.V. Landshoff and O. Natchmann, *Pomeron Physics and QCD*, (Cambridge University Press, 2002).
- [3] I.M. Dremin, Elastic scattering of hadrons, arXiv: 1206.5474 [hep-ph].
- [4] J. Kašpar V. Kunderát, M. Lokajíček and J. Procházka, Nucl. Phys. B **843**, 84 (2011).
- [5] R. Fiore, L. Jenkovszky, R. Orava, E. Predazzi, A. Prokudin, O. Selyugin, Int. J. Mod. Phys. A **24**, 2551 (2009).
- [6] G. Matthiae, Rep. Prog. Phys. **57**, 743 (1994).
- [7] M. Froissart, Phys. Rev. **123**, 1053 (1961).
- [8] A. Martin, Nuovo Cimento A **42**, 930 (1966).
- [9] L. Lukaszuk, A. Martin, Nuovo Cimento A **52**, 122 (1967).
- [10] A. Martin, AIP Conf. Proc. **1105** (2009), 258-261, arXiv:0812.0680 [hep-ph].
- [11] A. Martin, Phys. Rev. D **80**, 065013 (2009).

Table A1. Correlation coefficients from the correlation matrices associated with fit 1 and fit 2 results. The off-diagonal coefficients from fit 1 ($b_1 = b_2 = 0.5$ fixed) are displayed above the diagonal of the table (not filled) and those from fit 2, below that diagonal.

		fit 1							
	a_1	b_1	a_2	b_2	α	β	γ	s_h	K
fit 2	a_1	—	0.063	—	-0.990	-0.786	0.696	-0.929	0.558
	b_1	0.787	—	—	—	—	—	—	—
	a_2	0.208	0.026	—	-0.009	0.063	-0.073	0.027	0.271
	b_2	0.176	0.020	0.976	—	—	—	—	—
	α	-0.077	0.457	-0.063	-0.059	0.852	-0.770	0.968	-0.510
	β	0.061	-0.062	-0.005	-0.008	-0.139	-0.987	0.954	-0.304
	γ	-0.139	-0.131	0.041	0.039	0.178	-0.816	-0.899	0.247
	s_h	-0.252	-0.129	0.063	0.062	0.557	0.364	0.120	-0.424
	K	0.382	0.317	-0.206	-0.266	0.029	0.014	-0.031	-0.057

- [12] T.T. Wu, A. Martin, S.M. Roy, V. Singh, Phys. Rev. D **84**, 025012 (2011).
- [13] Ya.I. Azimov, Phys. Rev. D **84**, 056012 (2011).
- [14] Ya.I. Azimov, Froissart bounds for amplitudes and cross sections at high energies, arXiv: 1204.0984 [hep-ph].
- [15] Ya. Azimov, What is the real meaning of the Froissart theorem?, arXiv: 1208.4304 [hep-ph].
- [16] M. Giordano, E. Meggiolaro and N. Moretti, Asymptotic Energy Dependence of Hadronic Total Cross Sections from Lattice QCD, arXiv:1203.0961 [hep-ph].
- [17] G. Antchev *et al.* (TOTEM Collaboration), Europhys. Lett. **96**, 21002 (2011).
- [18] D.A. Fagundes, M.J. Menon, P.V.R.G. Silva, Braz. J. Phys. **42**, 452 (2012), arXiv:1112.4704v5 [hep-ph].
- [19] J. Beringer *et al.* (Particle Data Group), Phys. Rev. D **86**, 010001 (2012), <http://pdg.lbl.gov>.
- [20] U. Amaldi *et al.*, Phys. Lett. B **66**, 390 (1977).
- [21] C. Augier *et al.* (UA4/2 Collaboration), Phys. Lett. B **315**, 503 (1993).
- [22] P.R. Bevington and D.K. Robinson, *Data Reduction and Error Analysis for the Physical Sciences* (McGraw-Hill, Boston, Massachusetts, 1992).
- [23] R. Ulrich, R. Engel, S. Müller, F. Schüssler and M. Unger, Nucl. Phys. B (Proc. Suppl.) **196** 335 (2009).
- [24] R. Engel, T.K. Gaisser, P. Lipari and T. Stanev, Phys. Rev. D **58**, 014019 (1998).
- [25] R. Engel, Nucl. Phys. B (Proc. Suppl.) **82**, 221 (2000).
- [26] R.F. Ávila, E.G.S. Luna and M.J. Menon, Phys. Rev. D **67**, 054020 (2003).
- [27] Reference [19], <http://pdg.lbl.gov/2012/hadronic-xsections/hadron.html>
- [28] P. Abreu *et al.* (The Pierre Auger Collaboration), Phys. Rev. Lett. **109**, 062002 (2012).
- [29] J.R. Cudell *et al.* (COMPETE Collaboration), Phys. Rev. D **65**, 074024 (2002).
- [30] J.R. Cudell *et al.* (COMPETE Collaboration), Phys. Rev. Lett. **89**, N. 20, 201801 (2002).
- [31] J.R. Cudell, K. Kang and S.K. Kim, Phys. Lett. B **395**, 311 (1997).
- [32] E.G.S. Luna and M.J. Menon, Phys. Lett. B **565**, 123 (2003).
- [33] K. Igi and M. Ishida, Phys. Rev. D **66**, 034023 (2002).
- [34] K. Igi and M. Ishida, Phys. Lett. B **622**, 286 (2005).
- [35] M. Ishida and K. Igi, Prog. Theor. Phys. Suppl. **187**, 297 (2011).
- [36] M.M. Block and F. Halzen, Phys. Rev. D **70**, 091901 (2004).

- [37] M.M. Block and F. Halzen, Phys. Rev. D **72**, 036006 (2005).
- [38] M.M. Block and F. Halzen, Phys. Rev. Lett. **107**, 212002 (2011).
- [39] R.J. Eden, *High Energy Collisions of Elementary Particles* (Cambridge University Press, Cambridge, 1967), Sect. 7.1.
- [40] M.M. Block and R.N. Cahn, Rev. Mod. Phys. **57**, 563 (1985).
- [41] M.L. Goldberger, Y. Nambu and R. Oehme, Ann. Phys. (NY) **2**, 226 (1957).
- [42] P. Söding, Phys. Lett. **8**, 285 (1964).
- [43] F.W. Byron, Jr and R.W. Fuller, *Mathematics of Classical and Quantum Physics* (Dover Publications, New York, 1992), Chap. 6.
- [44] A. Alkin, J.R. Cudell, E. Martynov, Few Body Syst. **53**, 87 (2012), arXiv: 1109.1306 [hep-ph].
- [45] V. N. Gribov and A. A. Migdal, Yad. Fiz. **8**, 1002 (1968) [Sov. J. Nucl. Phys. **8**, 583 (1969)].
- [46] J. B. Bronzan, in Symposium on the Pomeron, Argonne National Laboratory, Report No. ANL/HEP-7327 (1973), p. 33.
- [47] J. D. Jackson, in 1973 Scottish Summer School, Report No. LBL-2079, 1973, p. 39.
- [48] J. B. Bronzan, G. L. Kane, and U. P. Sukhatme, Phys. Lett. **49B**, 272 (1974).
- [49] R.F. Ávila and M.J. Menon, Nucl. Phys. A **744**, 249 (2004).
- [50] M.J. Menon, A.E. Motter, B.M. Pimentel, Phys. Lett. B **451**, 207 (1999).
- [51] R.F. Ávila, E.G.S. Luna, M.J. Menon, Braz. J. Phys. **31**, 567 (2001); arXiv:hep-ph/0105065.
- [52] A. Donnachie, P. Landshoff, Phys. Lett. B **296**, 227 (1992);
- [53] R.J.M. Covolan, J. Montanha, K. Goulianos, Phys. Lett. B **389**, 176 (1996).
- [54] E. Martynov, J.R. Cudell, O.V. Selyugin, Eur. Phys. J. C **33**, S533 (2004).
- [55] J.R. Cudell, E. Martynov, O.V. Selyugin, A. Lengyel, Phys. Lett. B **587**, 78 (2004).
- [56] E. Martynov, J.R. Cudell, O.V. Selyugin, Ukr. J. Phys. **48**, 1272 (2003); arXiv:0307254[hep-ph].
- [57] R.F. Ávila and M.J. Menon, Extended Derivative Dispersion Relations, in *Sense of Beauty in Physics - A Volume in Honour of Adriano Di Giacomo*, edited by M. D'Elia et al. (Edizioni Plus - Pisa University Press, Pisa, Italy, 2006) pp. 153 - 158, arXiv:hep-ph/0601194.
- [58] R.F. Ávila and M.J. Menon, Braz. J. Phys. **37**, 358 (2007).
- [59] E. Ferreira and J. Sesma, J. Math. Phys. **49**, 033504 (2008).
- [60] K. Kang and B. Nicolescu, Phys. Rev. D **11**, 2461 (1975).
- [61] N.N. Khuri and T. Kinoshita, Phys. Rev. B **137**, 720 (1965).
- [62] URL: <http://root.cern.ch/drupal/>; <http://root.cern.ch/root/html/TMinuit.html>.
- [63] A. Achilli, Y. Srivastava, R. Godbole, A. Grau, G. Pancheri, O. Shekhovtsova, Phys. Rev. D **84**, 094009 (2011).
- [64] ATLAS Collaboration, Nat. Commun. **2**, 463 (2011), arXiv:1104.0326v1 [hep-ex].
- [65] A.J. Zsigmond (CMS Collaboration), arXiv:1205.3142v1 [hep-ex].
- [66] M.G. Poghosyan (for the ALICE collaboration), J. Phys. G **38**, 124044 (2011), arXiv:1109.4510v1 [hep-ex].
- [67] S.W. MacDowell and A. Martin, Phys. Rev. **135**, B 960 (1964).
- [68] D.A. Fagundes and M.J. Menon, Nucl. Phys. A **880**, 1 (2012), arXiv:1112.5115 [hep-ph].
- [69] Durham Reaction Database, <http://durpdg.dur.ac.uk/HEPDATA/REAC>.
- [70] A. Grau, S. Pacetti, G. Pancheri, Y.N. Srivastava, Phys. Lett. B **714**, 70 (2012).
- [71] P. Lipari and M. Lusignoli, Phys. Rev. D **80**, 074014 (2009).
- [72] D.A. Fagundes and M.J. Menon, Hadronic Cross Sections, Elastic Slope and Physical Bounds, in XII Hadron Physics, AIP Conf. Proc. **1520** (2013) pp. 297-299; arXiv:1208.0510 [hep-ph].
- [73] M.M. Block and F. Halzen, Phys. Rev. D **86**, 051504 (2012), arXiv 1208.4086 [hep-ph].
- [74] V.N. Gribov, A.A. Migdal, Sov. Phys. JETP **28**, 784 (1969).
- [75] M.G. Ryskin, A.D. Martin and V.A. Khoze, Diffractive Processes at the LHC, in Gribov-75 Memorial Workshop, Budapest, 2005, arXiv:hep-ph/0506272v1 (2005).
- [76] A. Achilli, R. Hegde, R.M. Godbole, A. Grau, G. Pancheri, Y.N. Srivastava, Phys. Lett. B **659**, 137 (2008).
- [77] A. Grau, R.M. Godbole, G. Pancheri, Y.N. Srivastava, Phys. Lett. B **682**, 55 (2009).

- [78] D.A. Fagundes, M.J. Menon, P.V.R.G. Silva, Reply to “Commentary on Total Hadronic Cross Section Data and the Froissart-Martin Bound by Fagundes, Menon and Silva”, arXiv:1211.3352v2 [hep-ph].
- [79] G. Antchev *et al.* (The TOTEM Collaboration), Europhys. Lett. **101**, 21003 (2013); CERN-PH-EP-2012-239.
- [80] G. Antchev *et al.* (The TOTEM Collaboration), Europhys. Lett. **101**, 21004 (2013); CERN-PH-EP-2012-353.
- [81] G. Antchev *et al.* (The TOTEM Collaboration), A luminosity-independent measurement of the proton-proton total cross-section at $\sqrt{s} = 8$ TeV, CERN-PH-EP-2012-354.
- [82] M.J. Menon, P.V.R.G. Silva, An updated analysis on the rise of the hadronic total cross-section at the LHC energy region, arXiv:1212.5096 [hep-ph].

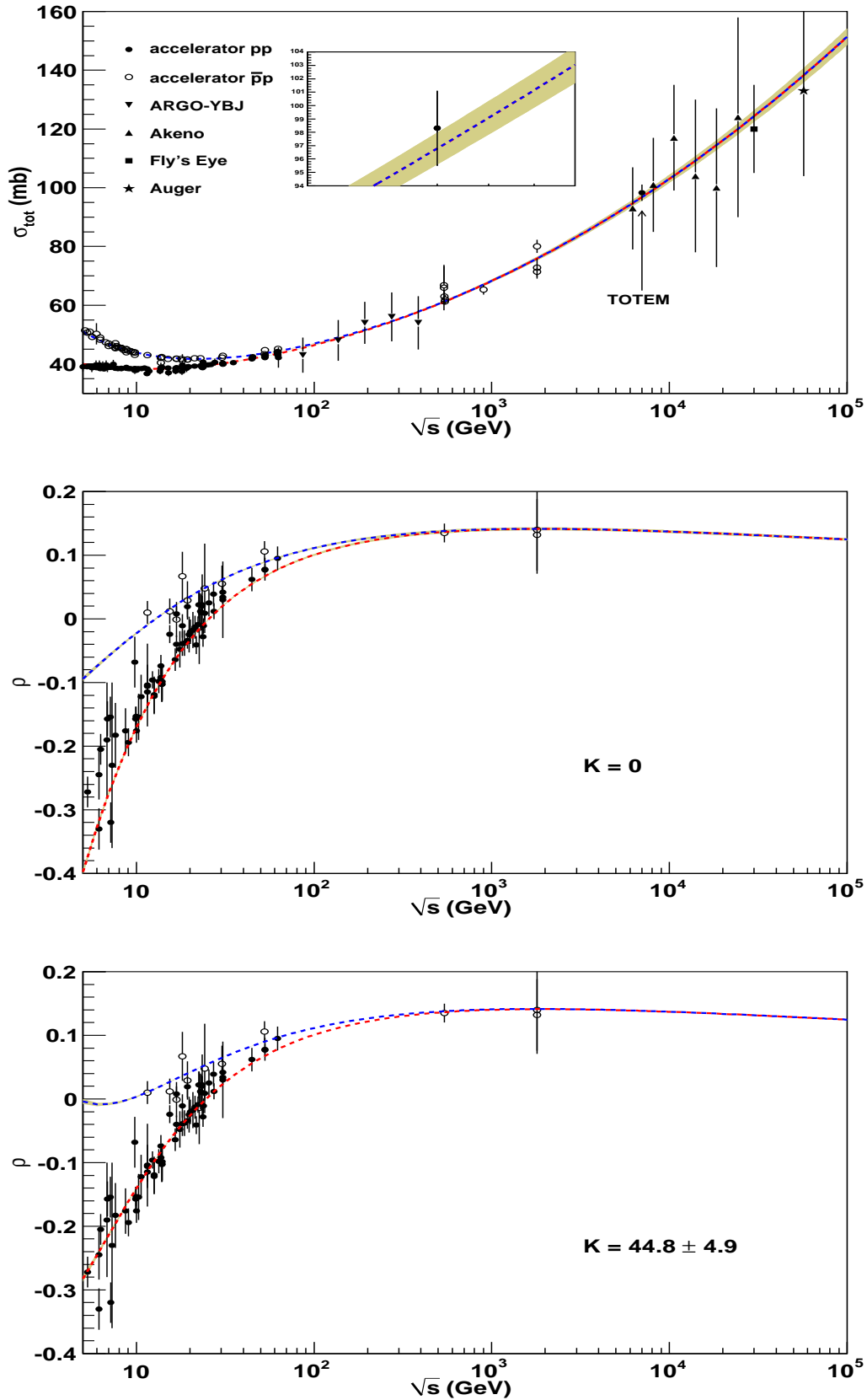


Figure 1. Individual fit to σ_{tot} data through parametrization (3-4) from fit 1 and predictions for $\rho(s)$ with $K = 0$ and K as a free fit parameter (table 1).

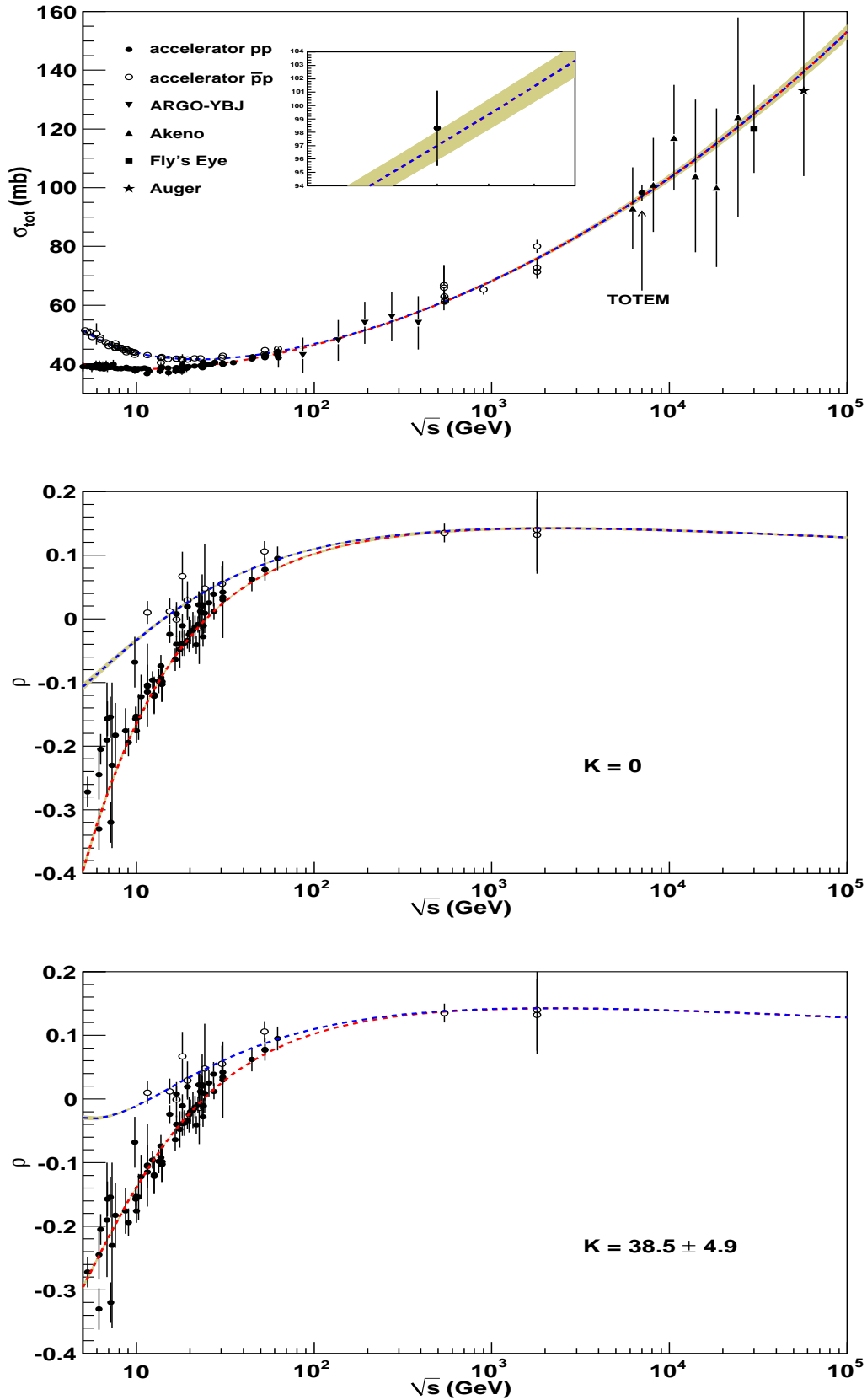


Figure 2. Individual fit to σ_{tot} data through parametrization (3-4) from fit 2 and predictions for $\rho(s)$ with $K = 0$ and K as a free fit parameter (table 1).

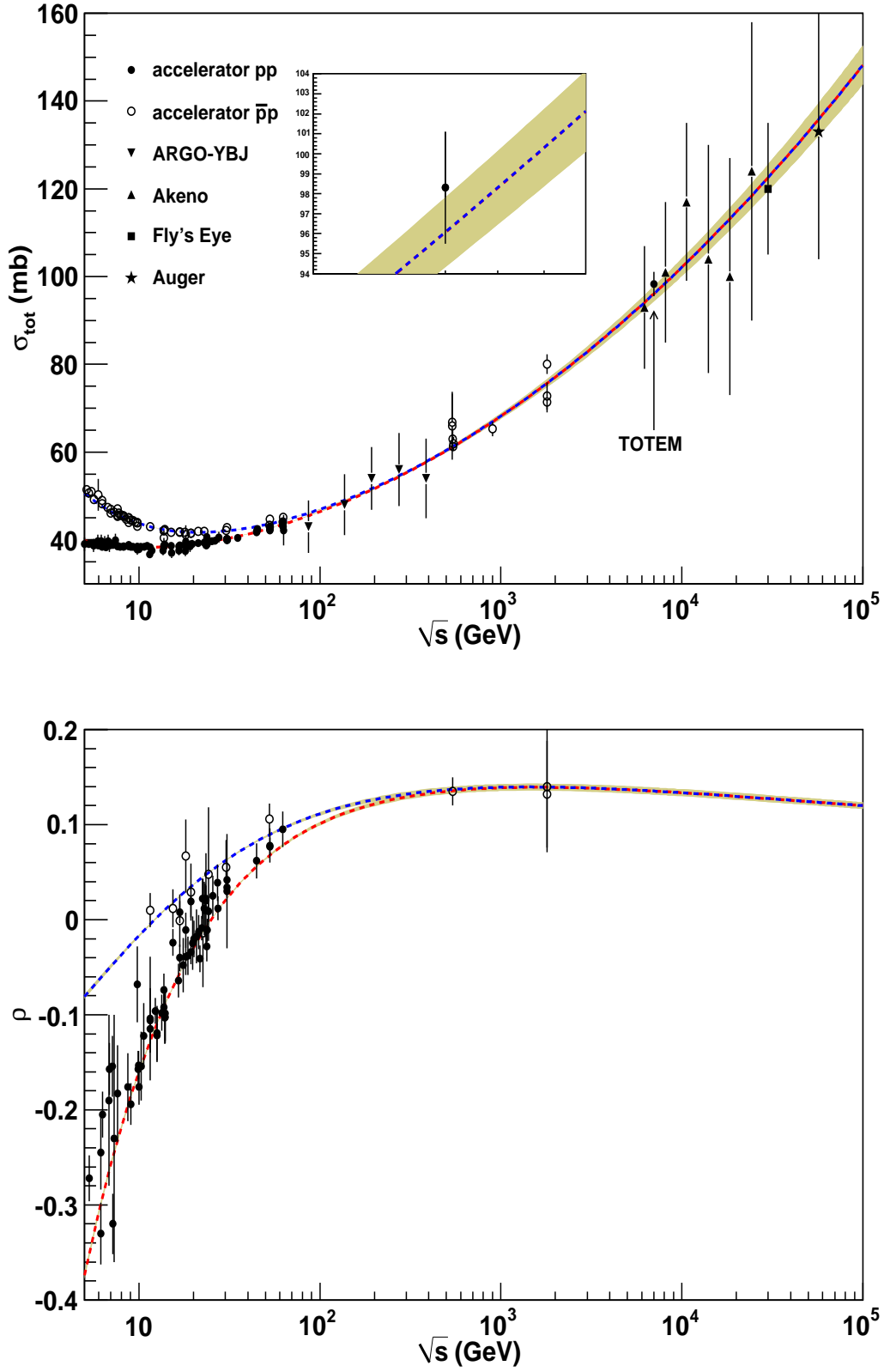


Figure 3. Simultaneous fits to σ_{tot} and ρ data from fit 1 and $K = 0$ (table 2).

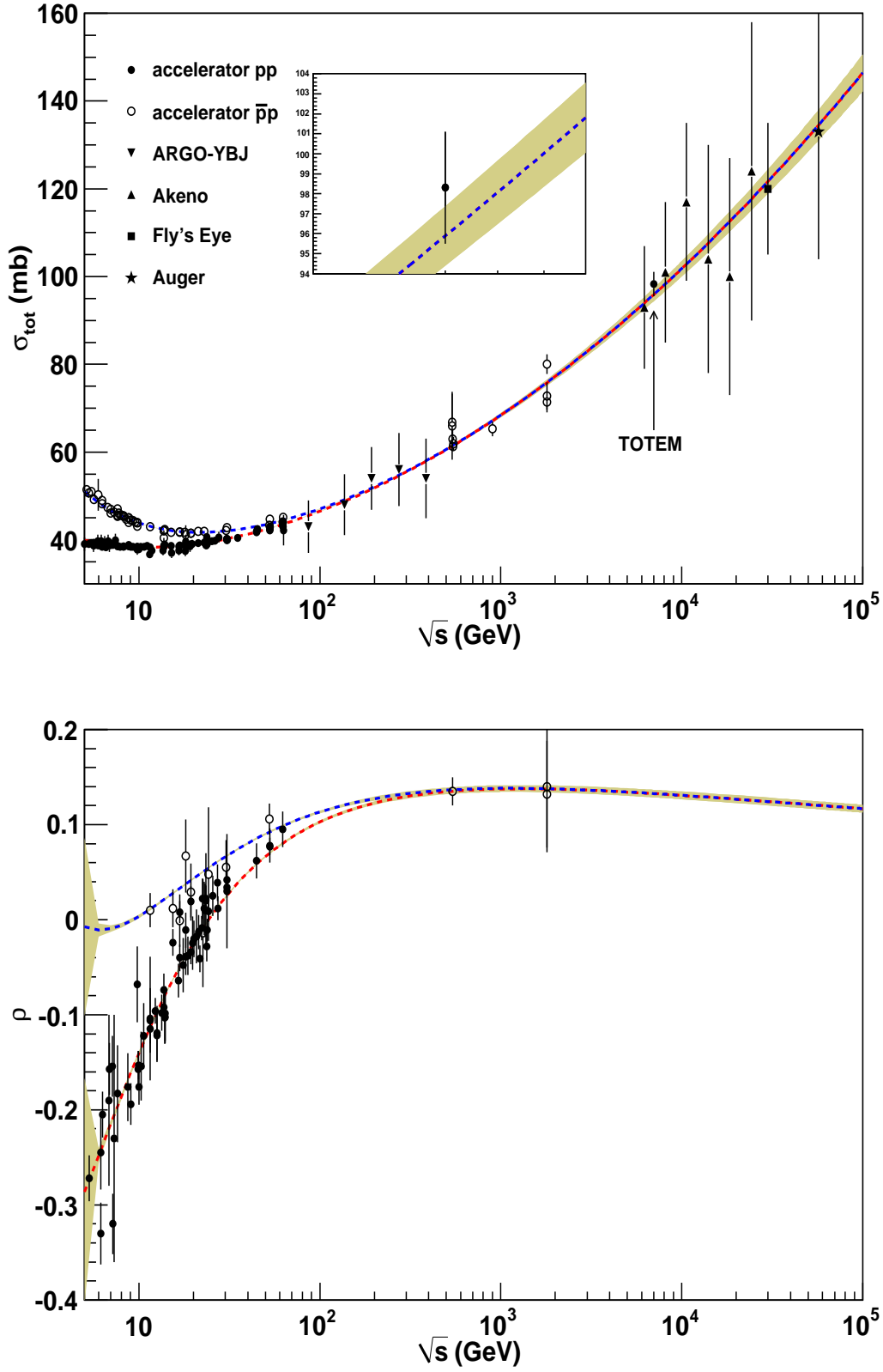


Figure 4. Simultaneous fits to σ_{tot} and ρ data from fit 1 and K as a free parameter (table 2).

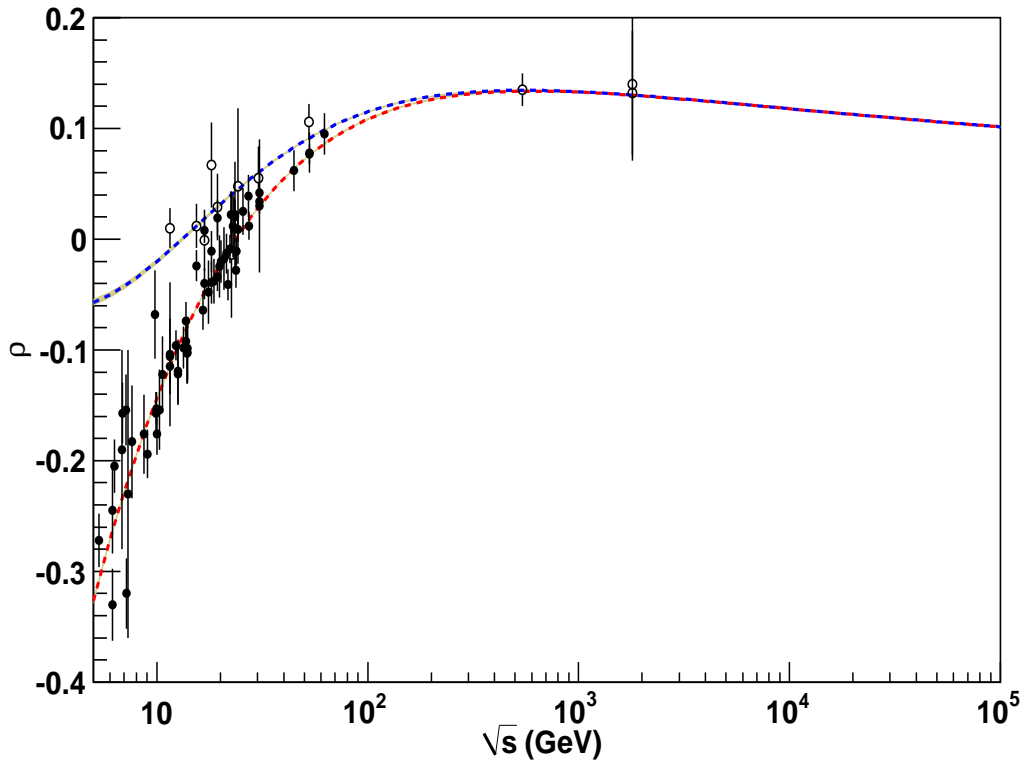
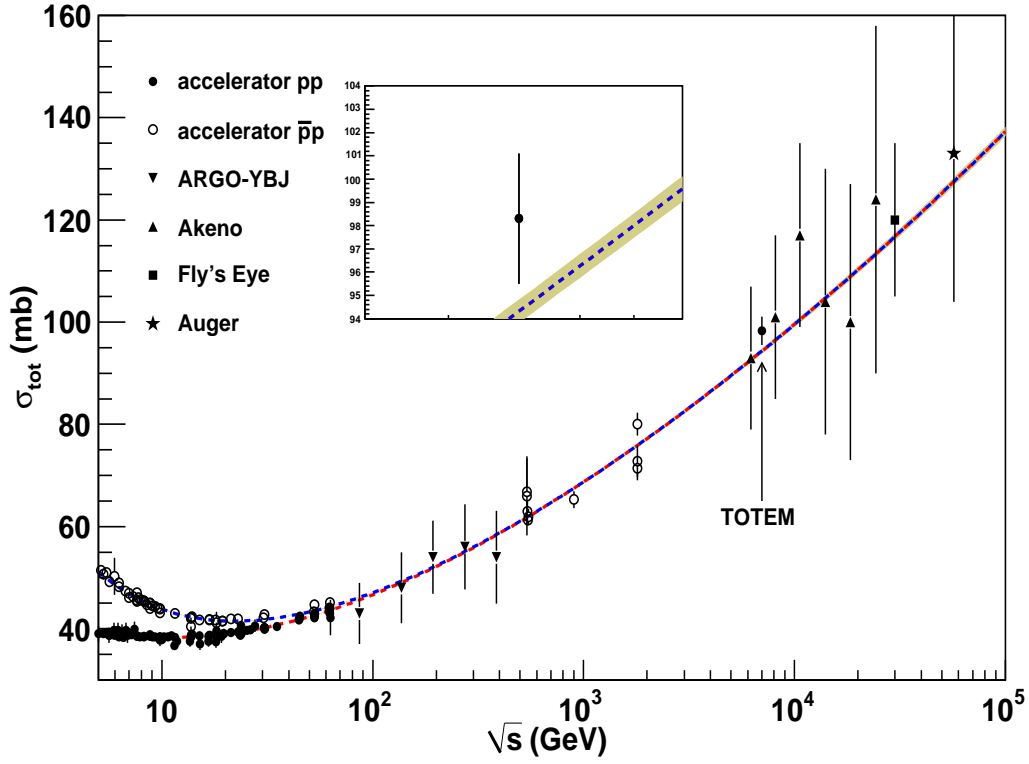


Figure 5. Simultaneous fits to σ_{tot} and ρ data from fit 2 and $K = 0$ (table 2).

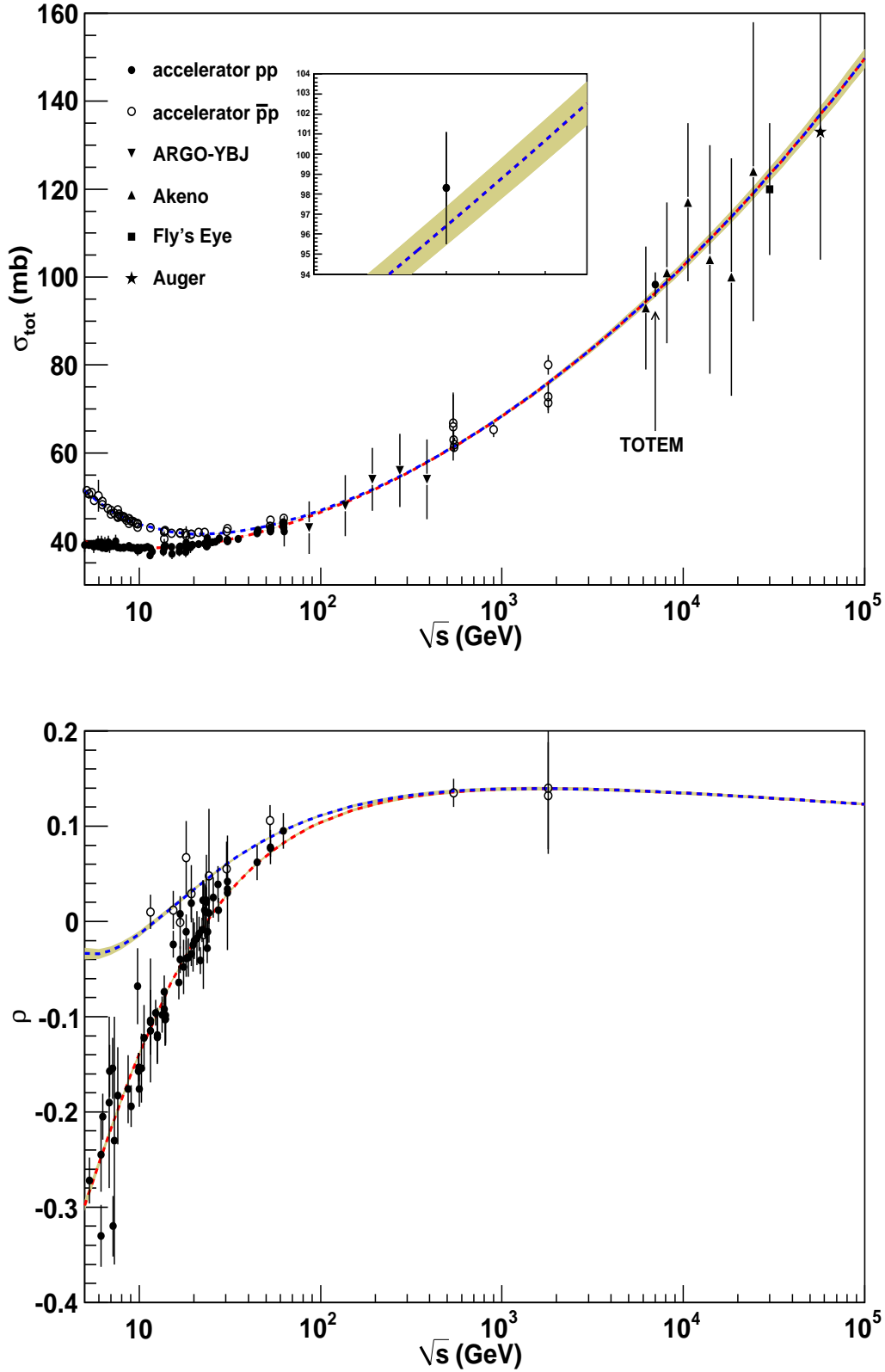


Figure 6. Simultaneous fits to σ_{tot} and ρ data from fit 2 and K as a free parameter (table 2).

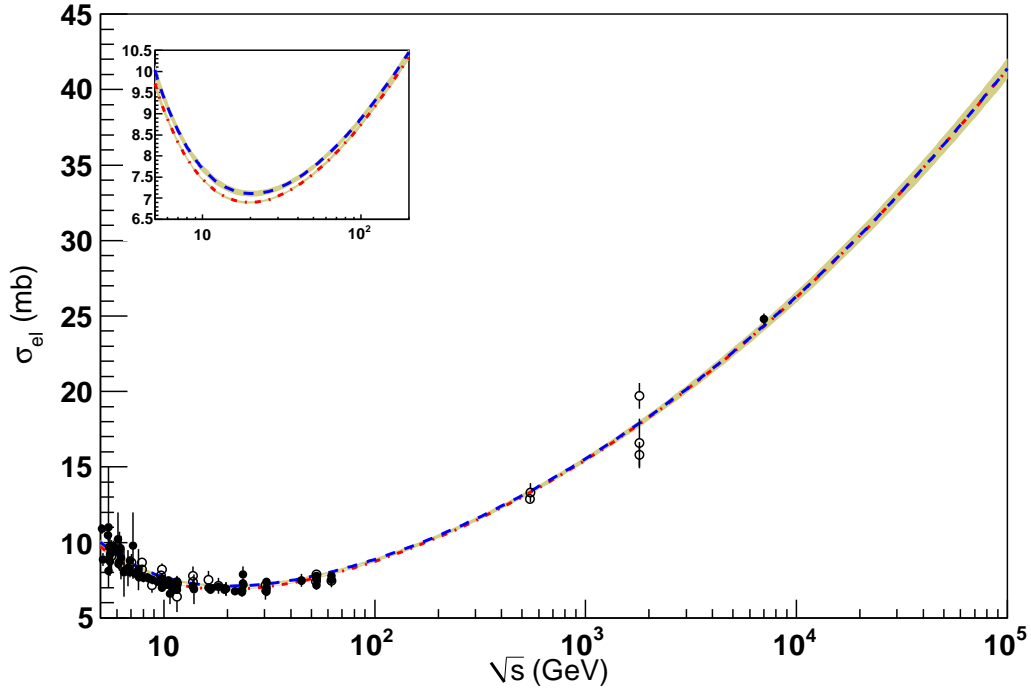


Figure 7. Fit result through parametrization (3-4) for the elastic cross section (table 3) and experimental data.

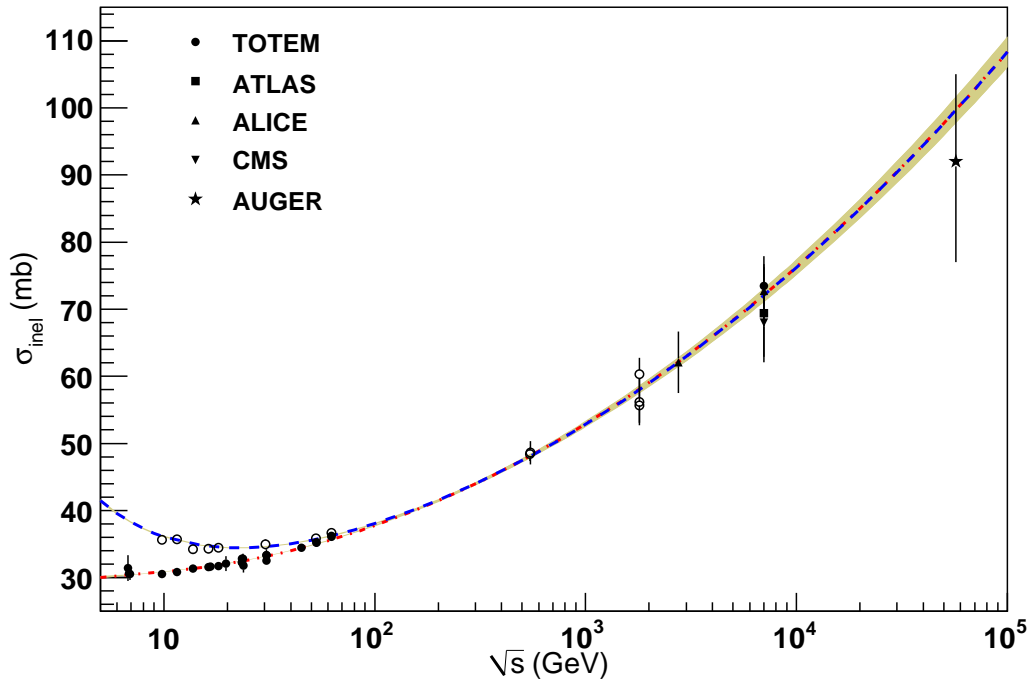


Figure 8. Predictions for the inelastic cross section and experimental data.

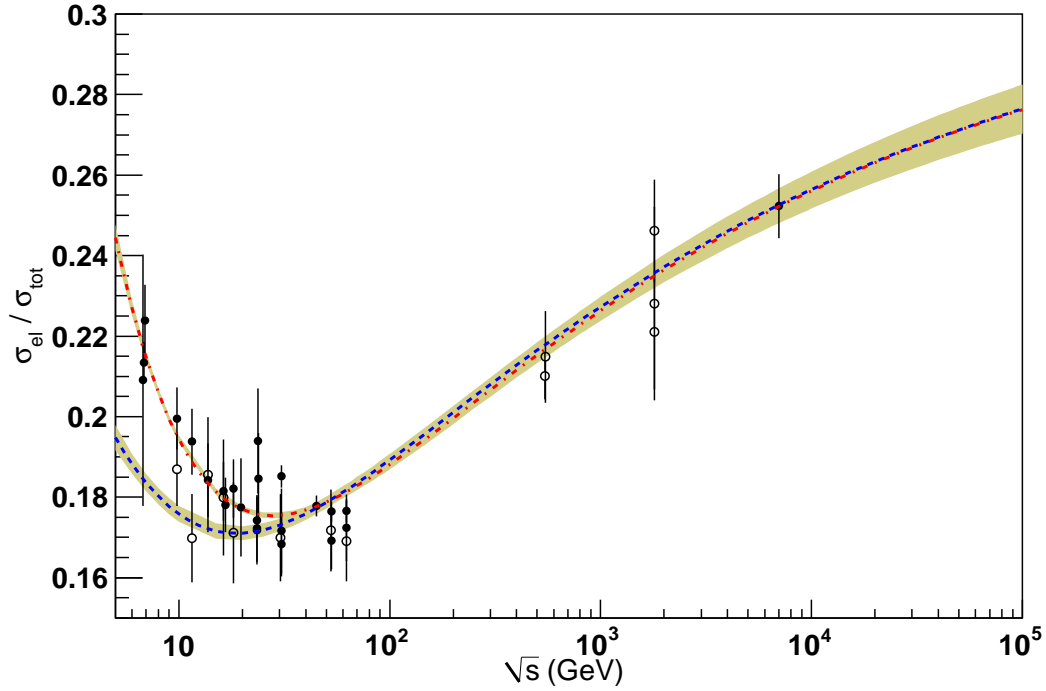


Figure 9. Predictions for the ratio between elastic and total cross section and experimental data.

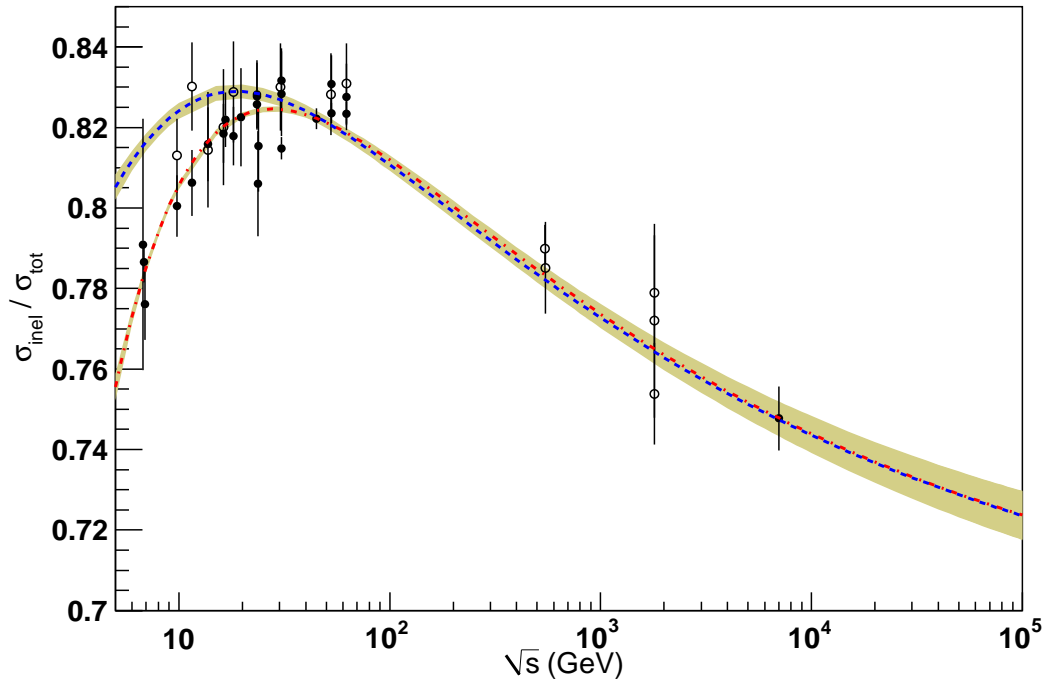


Figure 10. Predictions for the ratio between inelastic and total cross section and experimental data.

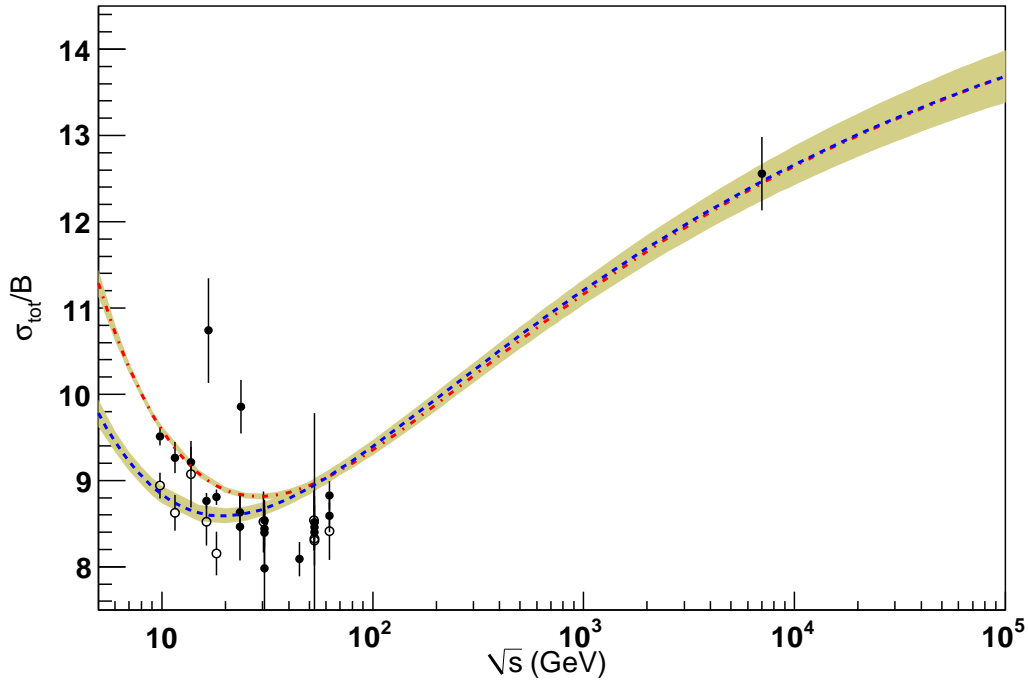


Figure 11. Predictions for the ratio between total cross section and the slope parameter and experimental data.

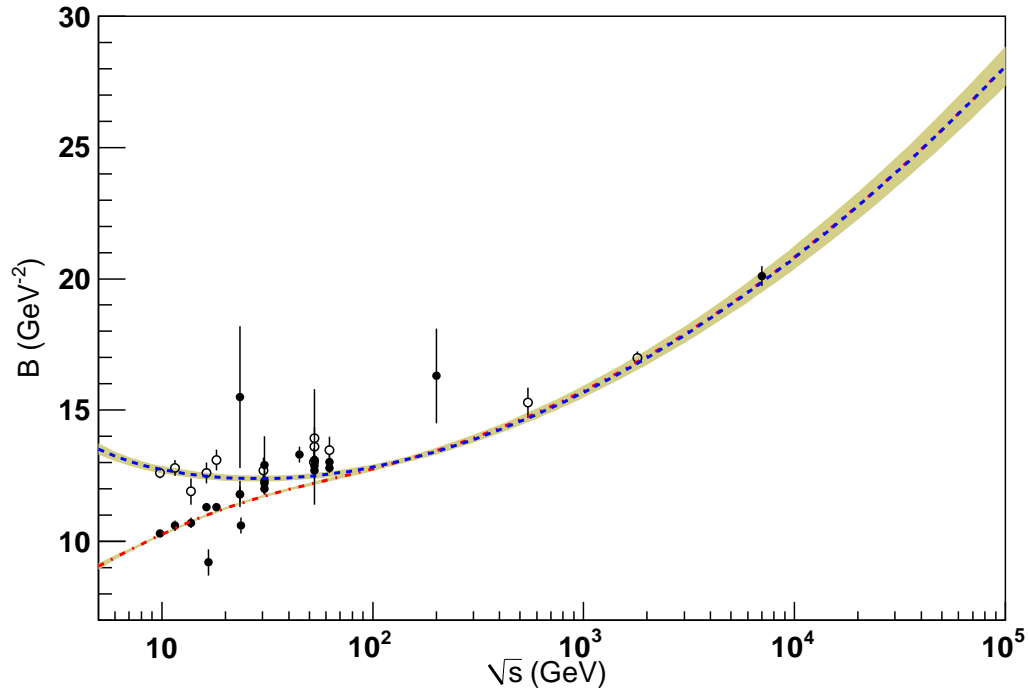


Figure 12. Predictions for the slope parameter and experimental data.